Congenital Malformations of the Head and Neck

7

Hee Jung Lee

Contents

H.J. Lee, M.D., M.P.H.
Department of Radiology, Dongsan Medical Center,
Keimynung University School of Medicine,
56 Dalsung Ro, Daegue, 700-712, Korea
e-mail: hjlee@dsmc.or.kr

I.-O. Kim (ed.), *Radiology Illustrated: Pediatric Radiology*, Radiology Illustrated,
DOI 10.1007/978-3-642-35573-8_7, © Springer-Verlag Berlin Heidelberg 2014

7.1 Introduction

Facial anomaly comprises anomalies of the nasolacrimal apparatus (nasolacrimal duct cyst), nasal cavity (choanal atresia, pyriform aperture stenosis), and nasofrontal region (dermoid cyst) (Lowe et al. 2000). Choanal atresia is rare, but it is the most common cause of congenital nasal obstruction. Congenital malformations of the neck can be classified as follows: embryonic remnants of thyroglossal duct (thyroglossal duct cyst, ectopic thyroid gland) or branchial apparatus (branchial sinus, branchial cyst, branchial fistula), thymopharyngeal duct anomalies, hypopharyngeal cysts (epiglottic cyst, vallecular cyst, laryngocele), foregut duplication cysts (enteric duplication cyst, bronchogenic cyst), and vascular malformations (lymphatic, venous) (Koeller et al. 1999; Sadler 2012; Som et al. 2003). Thyroglossal duct cyst is the most common congenital neck mass, while lymphatic malformation is the most common vascular malformation found in children. The anomalies arising from branchial apparatus show variable imaging and clinical features based on cyst, sinus, or fistula formation. The second branchial cleft cyst is the most common branchial apparatus anomaly. Most of the congenital neck masses are cystic in nature. However, ectopic thyroid gland and cervical thymus manifest as a mass mimicking a solid neoplasm of the neck. This chapter illustrates image findings of common congenital malformations of the head and neck in children by focusing on differential diagnosis.

7.2 Pathophysiology

Knowledge of the embryologic features and anatomy of the head and neck is essential for the evaluation of head and neck malformation. In addition, location and imaging findings of a lesion, clinical characteristics including the patient's age, and the presence of associated abnormality in the other sites of the body are helpful in differential diagnosis of congenital anomalies. The most common symptomatic clinical presentation is a sign of upper airway obstruction, especially for neonates and young infants.

Dermoid and epidermoid cysts are developmental cysts, typically located at the sites of embryologic fusion or the midline. Anomalies of thyroglossal ductal remnant occur at any site from the base of the tongue to the thyroid gland. Therefore, an anterior midline or paramedian cystic mass is typically a dermoid or thyroglossal duct cyst. Defect in branchial apparatus results in a wide spectrum of anomalies, which include fistulas, sinuses, cysts, and ectopic glands. Branchial cleft cyst is the most common branchial anomaly and can occur anywhere from the external auditory canal to the supraclavicular regions. Branchial cleft cysts and thymopharyngeal duct cysts are more laterally located and have characteristic positions in relation to the neck muscles and vessels. Lymphatic malformations are most commonly located in the posterior triangle of the neck and manifest as multiloculated cystic masses, which grow by insinuating around adjacent structures.

7.3 Imaging

The goal of imaging for head and neck malformation should be focused on arriving at an accurate diagnosis with minimizing radiation exposure, particularly for the thyroid glands of children. Plain radiography is usually indicated for the initial evaluation of children with acute respiratory symptoms, which can be caused by a mass in the hypopharynx or neck. Lateral views are more useful for evaluation of the airway. Ultrasonography (US) often allows accurate diagnosis of cystic neck lesions, beyond simply by distinguishing cystic from solid lesions. For example, a cystic lesion with "oil on water" or "lipid–fluid" level on US is suggestive of a dermoid cyst. Color Doppler also helps to detect abnormal vascularity associated with infectious lesions, solid components of tumors in cystic lesions, and vascular malformations. Computed tomography (CT) and magnetic resonance (MR) imaging are best suited for the evaluation of neck masses located within the deep neck spaces. The presence of intralesional calcification or bony structure can be better evaluated with CT than with MR. In addition, shorter CT scan duration has important advantages over MR in the emergency clinical setting. MR is the imaging modality of choice to evaluate head and neck masses with suspected intracranial extension. Fluoroscopy-guided barium swallowing esophagogram and sinogram are also indicated for the detection of sinus or fistular tract that are sometimes associated with branchial apparatus anomalies. Radioisotope scintigraphy is valuable for the evaluation of suspected thyroid gland abnormalities.

7.4 Spectrum of Congenital Head and Neck Malformations

7.4.1 Nasolacrimal Duct Cyst

Nasolacrimal duct cyst is caused by failure of canalization in the nasolacrimal duct. The lesion produces a lacrimal sac mucocele, and it manifests as a mass in the inferomedial canthus in neonates. CT and MR images depict a thin-walled cystic mass that extends from the inferomedial canthus to the nasal cavity, along with the course of the nasolacrimal duct (Fig. 7.1). Bilateral high-grade obstruction can lead to occlusion of the nasal aperture. The differential diagnosis includes dermoid or epidermoid cyst and naso-orbital cephalocele. Dermoid cyst is more frequently located in the superolateral wall of the orbit and rare in neonates.

Naso-orbital cephalocele shows a bony defect in the anterior skull and orbital wall (Lowe et al. 2000; Morón et al. 2004).

7.4.2 Choanal Atresia

Choanal atresia is caused by incomplete canalization of the choanae, and it results in obstruction or narrowing of the posterior nasal cavity. Choanal atresia is rare. However, it is the main cause of congenital nasal obstruction due to an anatomic obstruction in infants. Choanal atresia is classified as osseous, membranous, or osseomembranous, and partially osseous atresia is in about 90 % of cases. CT is the imaging modality of choice. Imaging features include narrowing of the posterior choanae to a width of less than 0.34 cm in children under 2 years old, inward bowing of the posterior maxilla, fusion or thickening of the posterior and inferior parts of the vomer, and the presence of a bone or soft tissue septum crossing the posterior choanae (Fig. 7.2). Many anomalies are associated with choanal atresia, with CHARGE syndrome (coloboma, heart malformation, choanal atresia growth and/or mental retardation, genital anomalies, ear anomalies) being the major developmental association (Lowe et al. 2000; Morón et al. 2004).

7.4.3 Pyriform Aperture Stenosis

Pyriform aperture stenosis is caused by premature fusion and overgrowth of the medial nasal processes, resulting in narrowing of the anterior nasal opening. CT scan depicts inward bowing and thickening of the nasal process of the maxilla and narrowing of the pyriform aperture less than 8 mm in width compared to a normal aperture, which is not less than 11 mm (Fig. 7.3). Many anomalies are also associated with pyriform aperture stenosis, including holoprosencephaly, facial hemangiomas, pituitary dysfunction, and central megaincisor (Lowe et al. 2000; Morón et al. 2004).

7.4.4 Dermoid Cyst and Epidermoid Cyst

Dermoid and epidermoid cysts are ectodermal inclusion cysts lined by squamous epithelium. They are developmental cysts, and unlike teratomas, they are not neoplasms. Epidermoid cyst is lined solely by squamous epithelium with internal keratin pearl, while dermoid cyst contains variable skin appendages of sebaceous glands, hair follicles, and sweat glands (Smirniotopoulos and Chiechi 1995). *Dermoid cyst* is typically located at the sites of embryologic fusion in frontozygomatic (orbital), sphenofrontal (nasal), sphenosquamosal (ear), and other calvarial sutures. Nasal dermoid cyst may be associated with a sinus tract that extends in the prenasal space to the foramen cecum through the anterior skull base. MR imaging is useful for tracing the tract into the cranium (Lowe et al. 2000; Morón et al. 2004). Orbital dermoid cyst is most commonly found in the upper outer quadrant or lacrimal fossa in more than 80 % of cases (Fig. 7.4). The floor of the mouth is the most common cervical location (Som et al. 2003) (Fig. 7.5). On US, dermoid cyst is a unilocular, cystic, or fatty mass in typical locations with or without pressure erosion (fossa formation) of the underlying bony cortex. They may show lipid material floating like supernatant "oil on water" over the heavier proteinaceous debris or "lipid–fluid" levels. Coalescence of fat into small nodules within the fluid matrix gives rise to the pathognomonic "sack of marbles" appearance on image findings. Epidermoid cyst is presumed to arise later in embryologic development than dermoid cyst, and it is typically lateral in location. Epidermoid cyst tends to be a unilocular and homogeneous cystic lesion. Unlike dermoid cyst, epidermoid cyst does not usually have the low attenuation values of fat. Occasionally, peripheral calcification and enhancement are present in epidermoid cyst (Fig. 7.6).

7.4.5 Thyroglossal Ductal Remnants

Thyroglossal duct forms a bridge between the base of the tongue and the thyroid gland, and the anomalies can be found at any level along its tract. Anomalies of thyroglossal duct remnants result from incomplete development (agenesis and hypoplasia), obliteration (thyroglossal duct remnant), or descent (ectopia) of the thyroglossal duct.

Thyroglossal duct cyst (TGDC) is the most common congenital neck lesion (70 %) in pediatric population. It is located most commonly at infrahyoid (65 %), followed by suprahyoid (20 %), and at the level of the hyoid bone (15 %). Uncomplicated TGDC typically represents as a hypoechoic nodule or cyst with a thin wall either in the midline of the anterior neck close to the hyoid bone (suprahyoid or hyoid) or paramedian (infrahyoid) within the strap muscles (Figs. 7.7, 7.8, and 7.9). CT demonstrates a well-circumscribed cyst with thin enhancing wall (Figs. 7.8 and 7.9). Internal content of the cyst can be variable depending on the presence of inflammation, hemorrhage, associated ectopic thyroid tissue, or malignancy. Enhancing solid nodule within the cyst may represent ectopic thyroid tissue, and calcifications within the solid nodule suggest an evolving papillary thyroid carcinoma (Som et al. 2003). The differential diagnosis of a midline neck mass includes dermoid cyst and lymph node. Unlike TGDC, there is no intimate relation with the hyoid bone, and these lesions typically are located superficial to the strap muscles.

Ectopic thyroid gland most commonly occurs as a lingual thyroid with variable sizes and contours. CT demonstrates typical high attenuation (>100 H.U) of thyroidal tissue by iodine content on preenhanced scan. The presence of a normal

functioning thyroid gland must be documented preoperatively by using US or radioisotope study (Koeller et al. 1999; Morón et al. 2004; Sadler 2012) (Figs. 7.10).

7.4.6 Branchial Apparatus Anomalies

Branchial apparatus anomalies are composed of a heterogeneous group of congenital malformations that arise from incomplete obliteration of pharyngeal clefts and pouches during embryogenesis (Sadler 2012; Som et al. 2003).

Each branchial apparatus has its arch separated by pouches on the internal endodermal side and by clefts on the external ectodermal side of the embryo. Branchial pouches are the Eustachian tube for the first arch, tonsillar fossa for the second arch, and pyriform sinus for the third and fourth arches. The first branchial apparatus has a persistent ectodermal cleft as the external auditory canal (EAC). The second, third, and fourth branchial clefts become enclosed in a common ectodermal-lined cavity called the cervical sinus of His, which appears along the anterior border of the sternocleidomastoid (SCM) muscle at the middle and lower third of the neck junction. The tissue between the endodermal pouch and the ectodermal cleft is mesoderm, and the mesoderm contains a dominant artery, nerve, cartilage, bone, and muscles. The endoderm of each pharyngeal pouch also gives rise to endocrine parenchyma of the parotid gland for the first arch, surface epithelium of the palatine tonsil for the second arch, and thymus and parathyroid glands for the third and fourth arches, respectively. Defect in branchial apparatus development results in fistulas, cysts, sinus tracts, ectopic glands, and cartilaginous remnants (Benson et al. 1992; Sadler 2012; Som et al. 2003).

A branchial cleft cyst is the most common branchial abnormality, which can occur anywhere from the EAC to the supraclavicular area. The cyst may contain internal air pockets in the presence of associated internal sinus or fistula tract.

The first branchial cleft cyst manifests as a cystic mass around the pinna and EAC (type I) or extending from the EAC to the angle of mandible (type II). A cyst may enlarge to present below the angle of the mandible or within or around the parotid gland (Fig. 7.11). The first branchial sinus tract may be present at the junction of the bone and the cartilage portion of the EAC.

The second branchial cleft cyst accounts for 80–90 % of branchial apparatus anomalies and manifests as a cyst typically located in the posterolateral to the submandibular gland, lateral to the carotid space, and anterior to the SCM muscle (Fig. 7.12). The second branchial sinus manifests as a tiny skin pit on the anterior border of the SCM muscle at the junction site of the middle and lower third of the neck, and the fistula tract may extend to the tonsillar fossa (Fig. 7.13).

The third branchial cleft cyst is located in the upper posterior cervical space or lower anterior neck (Fig. 7.14). *The fourth branchial cleft cyst* may be located anterior to the aortic arch on the left or anterior to the subclavian artery on the right (Figs. 7.15 and 7.16). The third and fourth branchial sinus or fistula may manifest as recurrent thyroiditis. Esophagogram or sinogram may reveal a sinus or a fistula tract between the pyriform sinus and the skin pit in the lower anterior neck or adjacent to the anterior left thyroid lobe (Benson et al. 1992; Koeller et al. 1999; Som et al. 2003) (Fig. 7.17).

7.4.7 Thymic Anomalies

Thymic primordia arise from the third and fourth pharyngeal pouches. Spectrum of anomalies may occur anywhere along the thymopharyngeal duct into the mediastinum, resulting in failure of descent (cervical thymus), sequestration (ectopic thymus), or failure to obliterate (thymic cyst) (Sadler 2012). The majority of these anomalies are seen on the left side of the neck.

Cervical thymus is usually located lateral to the carotid sheath and anterior to the SCM muscle. US demonstrates a solid, homogeneous, and hypoechoic mass anterior to the SCM muscle and extending inferiorly from the angle of the mandible. Color Doppler image shows minimal vascular flow within the mass. MR demonstrates a well-circumscribed homogeneous mass with slight hypointensity on T1-weighted image, mild hyperintensity on T2-weighted image, and minimal enhancement after contrast enhancement. The mass does not invade or compress adjacent structures (Nasseri and Eftekhari 2010) (Fig. 7.18). *Ectopic thymus* may be seen occasionally in the thyroid gland (Gimm et al. 1997) (Fig. 7.20). *Thymic cyst* is rare in children and located at the anterior cervical triangle on the left side, along the anterior margin of the SCM muscle extending or without extending into the anterior mediastinum. The cyst is unilobular or multilobular and may contain clear or complicated fluid (Cigliano et al. 2007).

7.4.8 Hypopharyngeal Cysts

A variety of terms have been used for cysts arising from the tongue base and hypopharynx based on their sites of origin, such as an epiglottic cyst, vallecular cyst (Figs. 7.22 and 7.23), or laryngeal cyst. Laryngocele is an air- or fluid-filled outpouching of the laryngeal saccule that communicates with the laryngeal ventricle (Fig. 7.24). Two pathogeneses have been proposed on their developmental origin, which are retention cysts as obstruction of mucus glands and embryological malformation arising from the fourth to sixth branchial arches. Most of the affected infants are presented with inspiratory stridor or symptoms of upper airway obstruction. US demonstrates a unilocular, thin-walled cyst

in the hypopharynx. MR is the diagnostic modality of choice for evaluation of the exact location. The signal intensity of the cysts is usually high on T2-weighted image and variable on T1-weighted image, depending on whether the cysts are filled with fluid, proteinaceous debris, or air (Chung et al. 2004; Suzuki et al. 2011).

7.4.9 Foregut Duplication Cysts

The primitive foregut gives rise to the oropharynx, the lower respiratory system, and the esophagus. Therefore, the foregut duplication cysts include enteric duplication cyst and bronchogenic cyst based on their epithelial lining (Sadler 2012). Most foregut cysts manifest during the first year of life, and the affected infants present with respiratory distress due to airway obstruction. The most common site of foregut duplication cysts in the head and neck is the oral cavity (Kieran et al. 2010) (Fig. 7.25). They can also occur along the course of the trachea and esophagus, and usually do not communicate with the trachea or esophagus (Fig. 7.26). US is very useful in demonstrating superficial cysts. The typical US appearance of enteric duplication cysts is that of a thick-walled cyst with or without a "double wall" sign, which consisted of an inner echogenic mucosal and outer hypoechogenic muscle layers, as in enteric duplication cysts arising from the other gastrointestinal tract. MR is preferred for the evaluation of its relationship with the trachea or esophagus. The differential diagnosis includes variable cysts according to their locations, such as dermoid cyst or TDGC in the tongue base and hypopharyngeal or branchial cleft cyst in the lateral neck.

7.4.10 Vascular Malformations

Vascular malformations are classified as arteriovenous, capillary, venous (cavernous hemangiomas), lymphatic (lymphangiomas or cystic hygromas), or combined, based on their lining endothelium. Vascular malformations, unlike hemangiomas, do not show neoplastic endothelial proliferation (Mulliken and Glowacki 1982).

Lymphatic malformation develops from lymphatic sacs that fail to communicate with the remaining lymphatic system. The lesion is the most common vascular malformation among young children. Lymphatic malformation is commonly located in the posterior triangle of the neck, lower portion of the face, and axilla in the first 2 years of life. MR is the best modality to demonstrate the extent of the lesion. Macrocystic lymphatic malformation (cystic hygroma) has characteristic imaging features including multiseptated cystic mass that grows by insinuating around adjacent structures (Figs. 7.27 and 7.29). Depending upon the presence of internal hemorrhage, there may be fluid–fluid levels and variable signal intensity of the cysts on MR (Fig. 7.28). Lack of wall thickening or enhancement and absence of phleboliths differentiate lymphatic from venous malformations (Koeller et al. 1999; Morón et al. 2004; Som et al. 2003).

Venous malformation manifests in both children and adults, grows proportionate to the child, and does not regress spontaneously. Venous malformation frequently affects the oral cavity, skeletal muscles of the head and neck involving the masseter, pterygoid, trapezius, and SCM muscles. Imaging findings are variable according to their endothelial vessels. US can suggest the diagnosis of a venous malformation by demonstrating a multilocular mass with fluid-filled spaces or fluid–debris levels. Doppler US may not be able to demonstrate flow in the lesion, since venous malformation is a low-flow lesion. The characteristic imaging feature of venous malformation is the presence of phleboliths as laminated calcific densities on CT. The enhancement is initially heterogeneous, becoming more homogeneous on delayed images. MR imaging demonstrates a hyperintense mass of venous lakes on T2-weighted images, with occasional septation and variable enhancement (Fig. 7.30). Phleboliths appear as a focal signal void on both T1- and T2-weighted images (Baker et al. 1993; Som et al. 2003).

7.5 Illustrations: Congenital Malformations of the Head and Neck

7.5.1 Nasolacrimal Duct Cyst

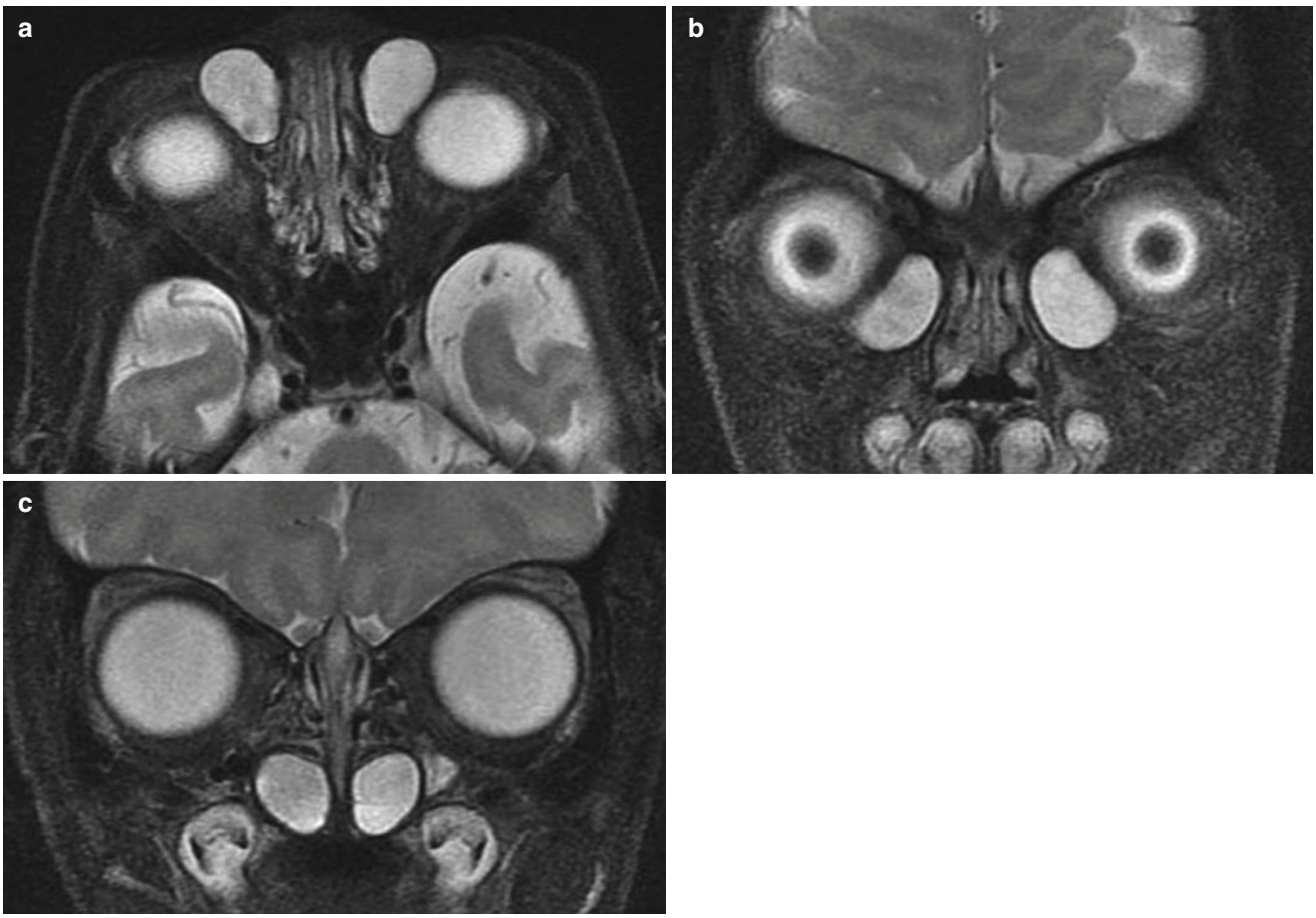

Fig. 7.1 Nasolacrimal duct cysts in a 15-day-old girl. (**a**) Axial T2-weighted image shows cystic masses in the medial canthus of both the orbits. (**b**, **c**) Coronal T2-weighted images show the cystic masses extending from the medial canthus into the nasal cavities along the nasolacrimal ducts

7.5.2 Choanal Atresia

Fig. 7.2 Choanal atresia in a neonate. Axial CT scan with a bone window shows narrowing of both choanae, thickening of the posterior and inferior parts of the vomer, and the presence of an air–fluid level in the left nasal cavity due to choanal obstruction. He also had bilateral external auditory canal atresia

7.5.3 Pyriform Aperture Stenosis

Fig. 7.3 Pyriform aperture stenosis in a 1-month-old infant. Axial CT scan shows inward bowing of the nasal process of the maxilla and narrowing of the anterior nasal cavity (*arrow*)

7.5.4 Dermoid and Epidermoid Cysts

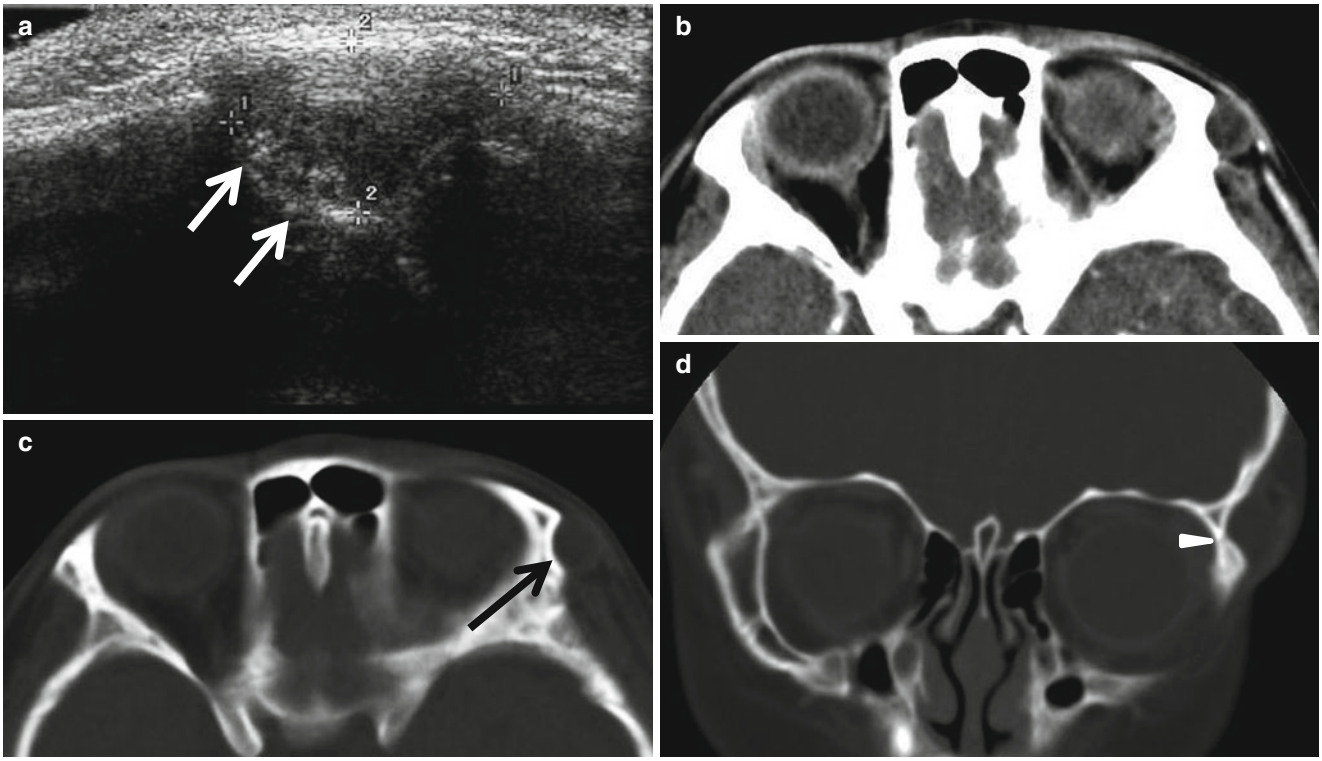

Fig. 7.4 Orbital dermoid cyst in a 5-year-old girl. (**a**) US shows an oval-shaped nodule with internal echogenic foci in the superolateral wall of the orbit. The underlying bony cortex of the orbital rim produces the appearance of a fossa (*arrows*). (**b**) Contrast-enhanced axial CT scan shows a round fatty mass in the superolateral aspect of the left orbit. (**c**, **d**) Axial and coronal CT scans of bone window show osseous scalloping that produces the appearance of a fossa (*arrow*) with a sclerotic margin near the zygomaticofrontal suture (*arrowhead*)

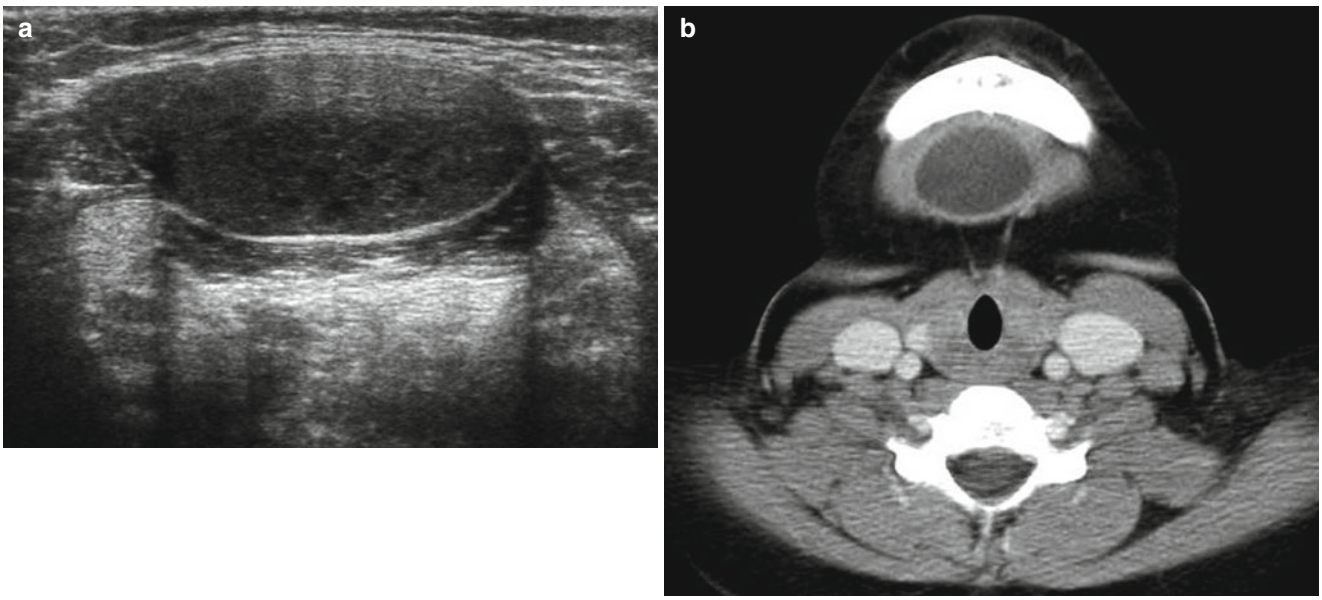

Fig. 7.5 Submental dermoid cyst in a 10-year-old boy. (**a**) US shows a hypoechogenic cystic mass with internal echogenic lobules and foci. (**b**) Contrast-enhanced axial CT scan shows a round cystic mass in the midline tongue base. The differential diagnosis includes thyroglossal duct cyst, dermoid cyst, cystic teratoma, and enteric duplication cyst

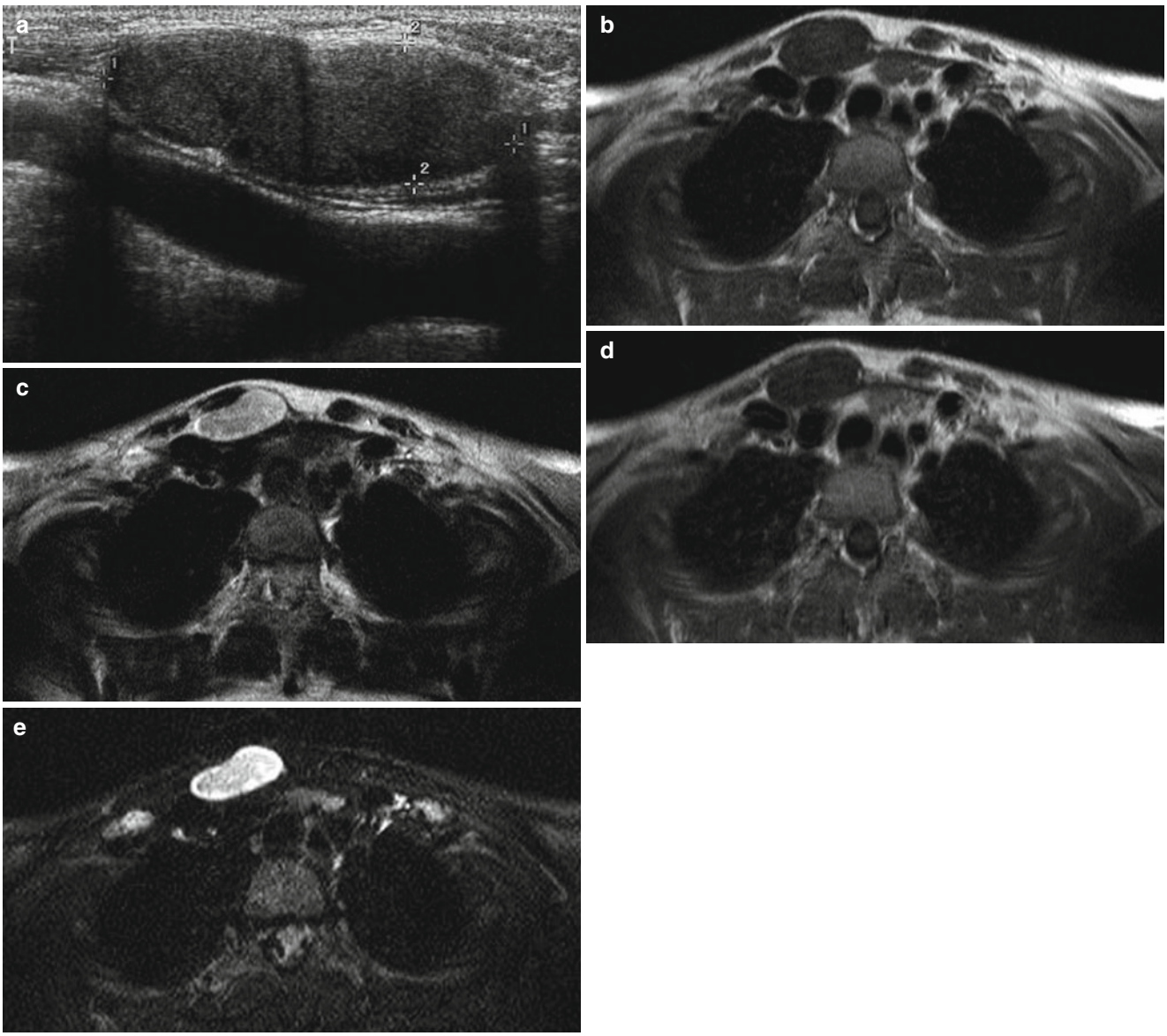

Fig. 7.6 Epidermoid cyst in a 10-year-old girl. (**a**) US shows a bilobed hypoechoic lesion in the region of the right sternoclavicular junction. Note the internal echogenic foci. (**b**–**d**) The mass appears as isosignal intensity on T1-weighted image (**b**) and slightly high signal intensity on T2-weighted image (**c**) and demonstrates no contrast enhancement (**d**). (**e**) Diffusion-weighted image shows bright high signal intensity of the lesion

7.5.5 Thyroglossal Duct Remnants

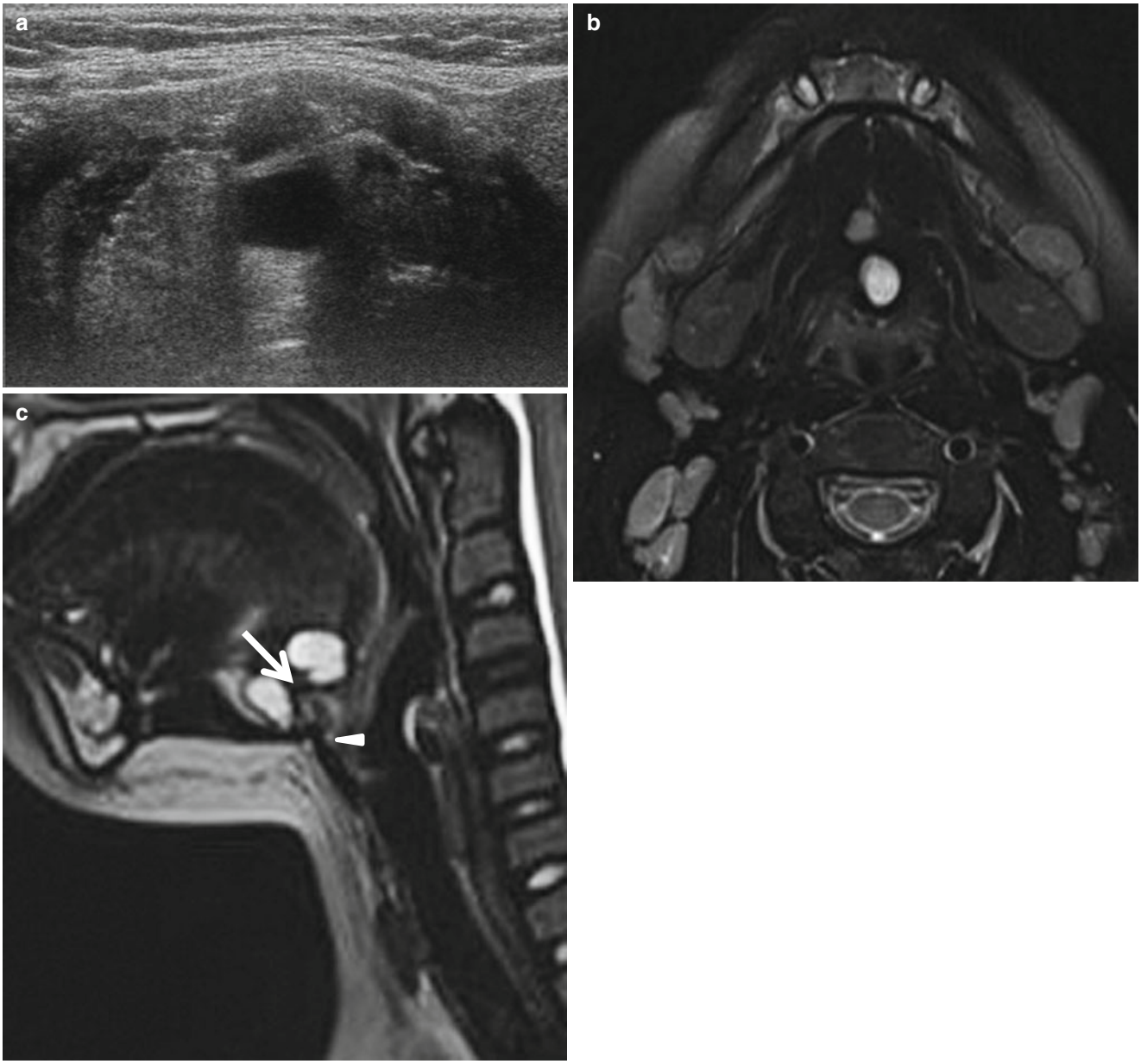

Fig. 7.7 Suprahyoid thyroglossal duct cyst in a 9-year-old boy. (**a**) US shows a bilocular cystic lesion in the midline aspect of the preepiglottic region. (**b**) Axial T2-weighted image shows a bilobed cystic mass of high signal intensity in the midline tongue base. (**c**) Sagittal T2-weighted image shows a fine tract (*arrow*) between the cystic locules and the relationships between the cyst and the hyoid bone (*arrowhead*)

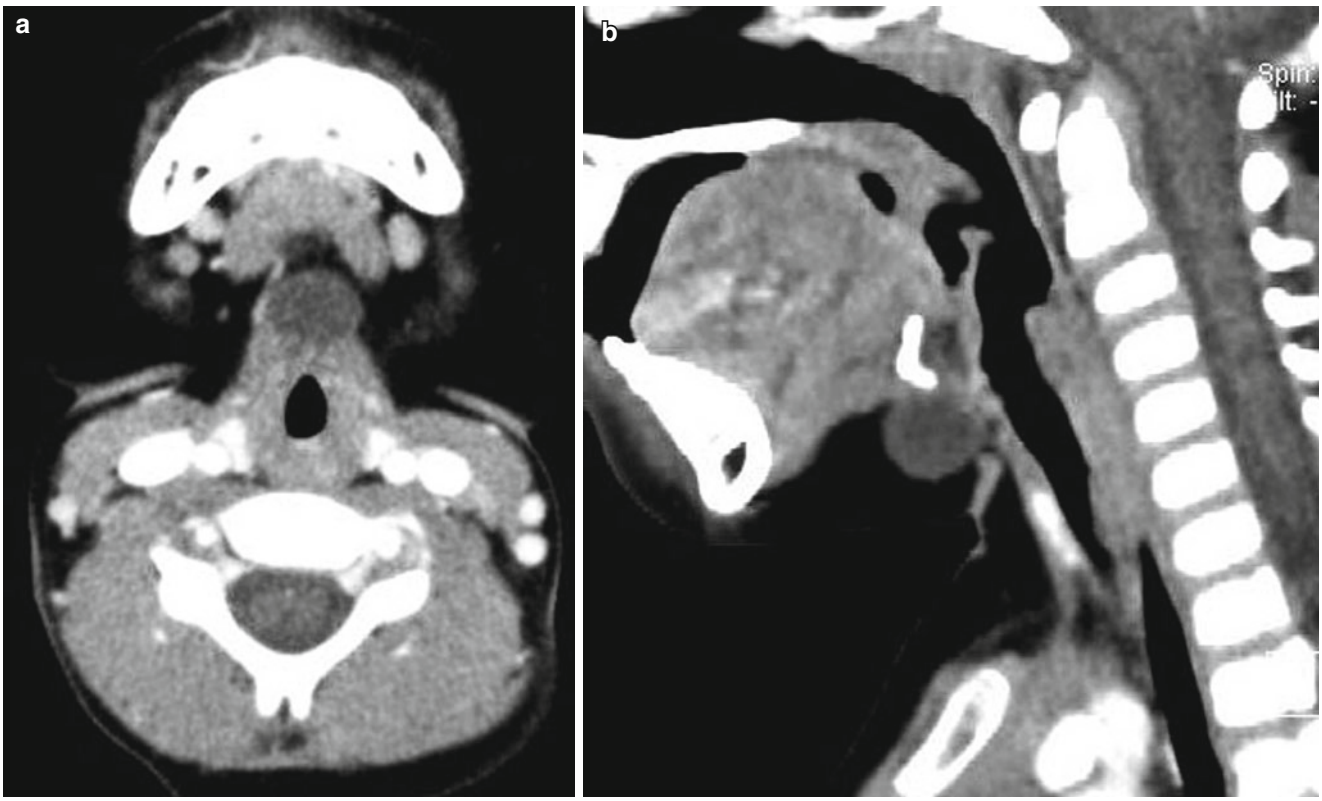

Fig. 7.8 Thyroglossal duct cyst on the level of the hyoid bone in a 3-year-old boy. (**a**) Contrast-enhanced axial CT scan shows a round midline cyst in the submental space. (**b**) Sagittal reformatted CT scan shows a well-defined unilocular, thin-walled cyst abutting the hyoid bone

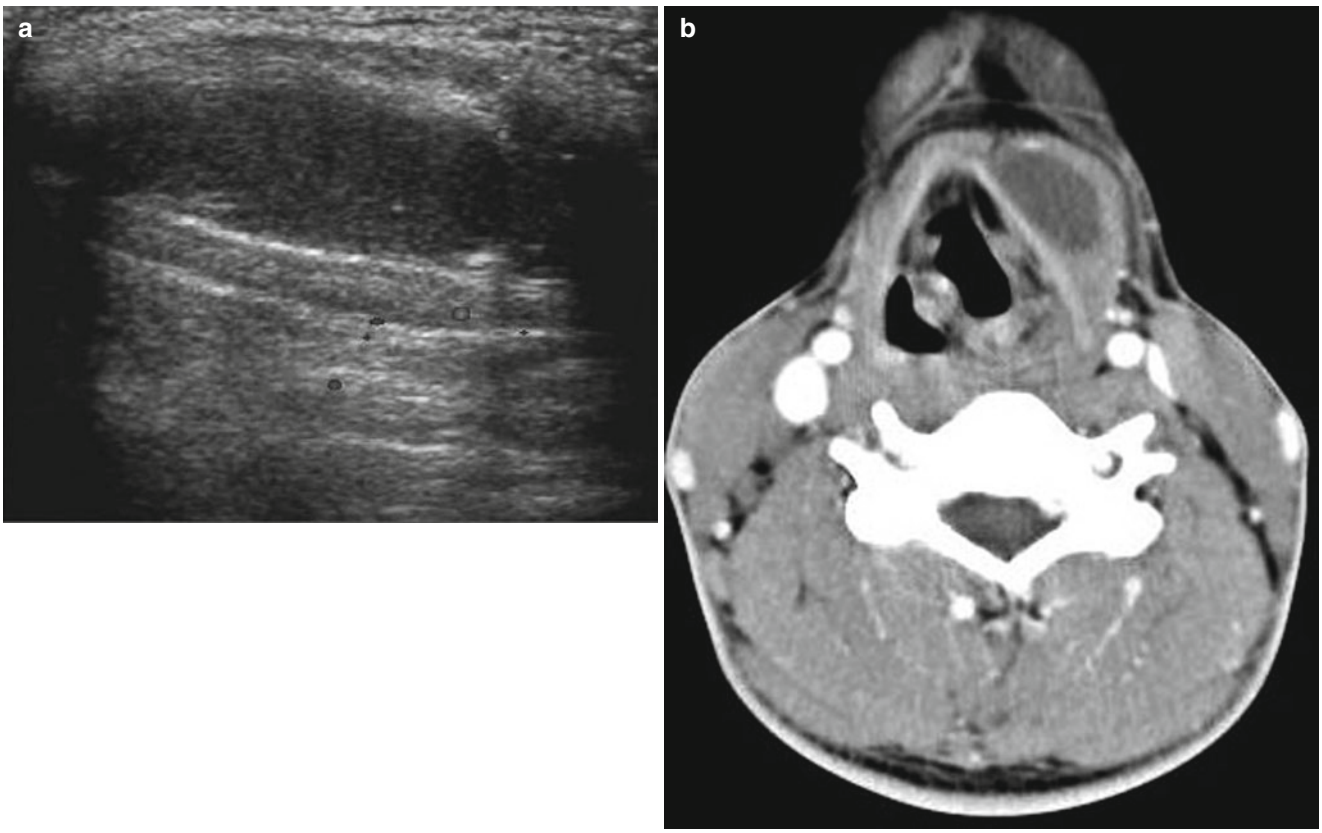

Fig. 7.9 Infrahyoid thyroglossal duct cyst in a 15-year-old boy. (**a**) US shows a hypoechoic cystic mass embedded in the left strap muscle. (**b**) Contrast-enhanced axial CT scan shows a well-defined unilocular, thin-walled cyst embedded in the left strap muscle

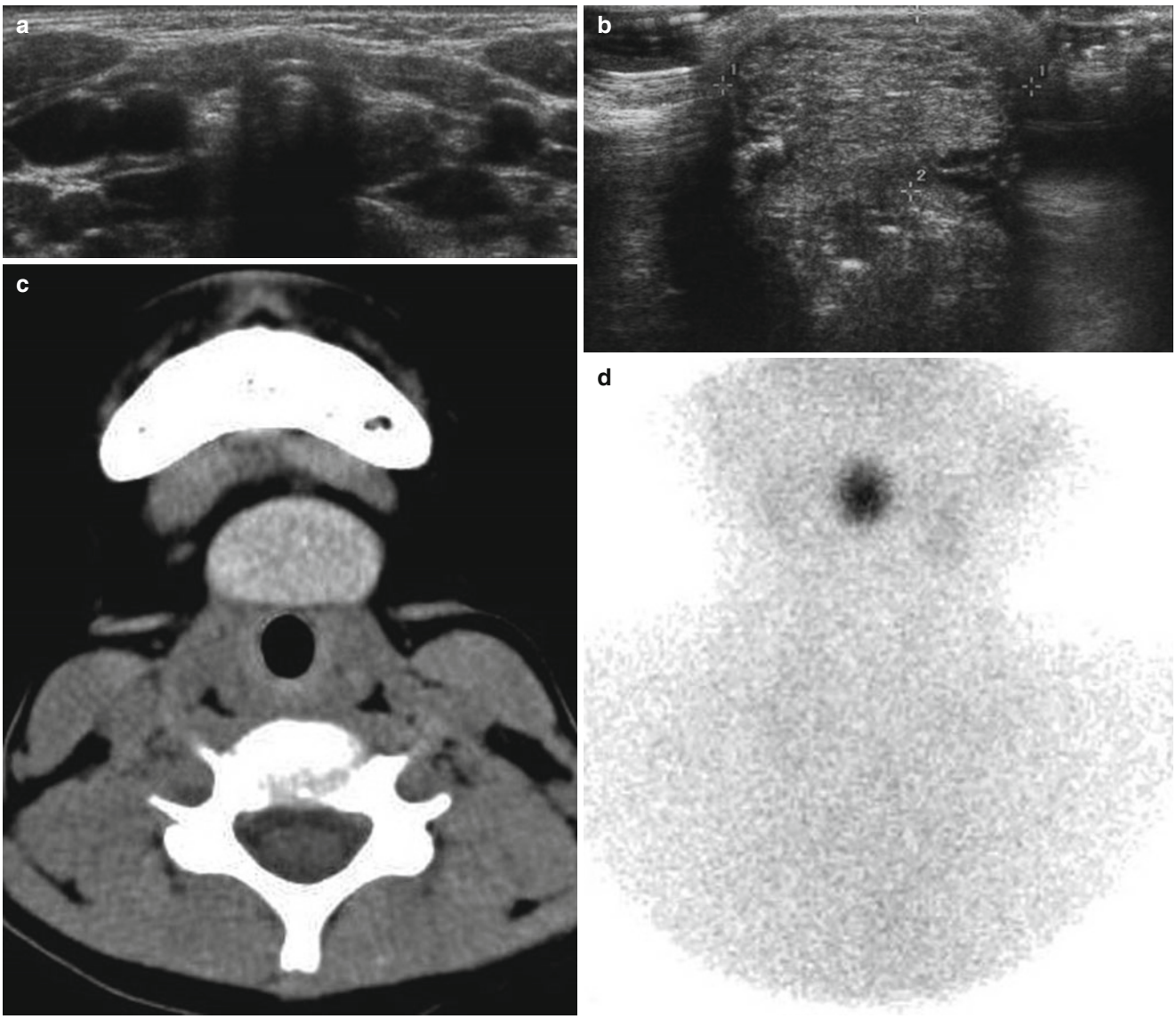

Fig. 7.10 Ectopic thyroid gland in a 7-year-old girl. (**a**) US shows absence of the thyroid gland at the low neck. (**b**) US obtained at the level of the hyoid bone shows a heterogeneous echogenic solid mass. (**c**) Precontrast axial CT scan shows hyperattenuated ectopic thyroid tissue at the level of the hyoid bone. (**d**) Tc-99m radionuclide scan shows an ectopic lingual thyroid gland and no uptake of the radioisotope at the normal location of the thyroid gland

7.5.6 Branchial Apparatus Anomalies

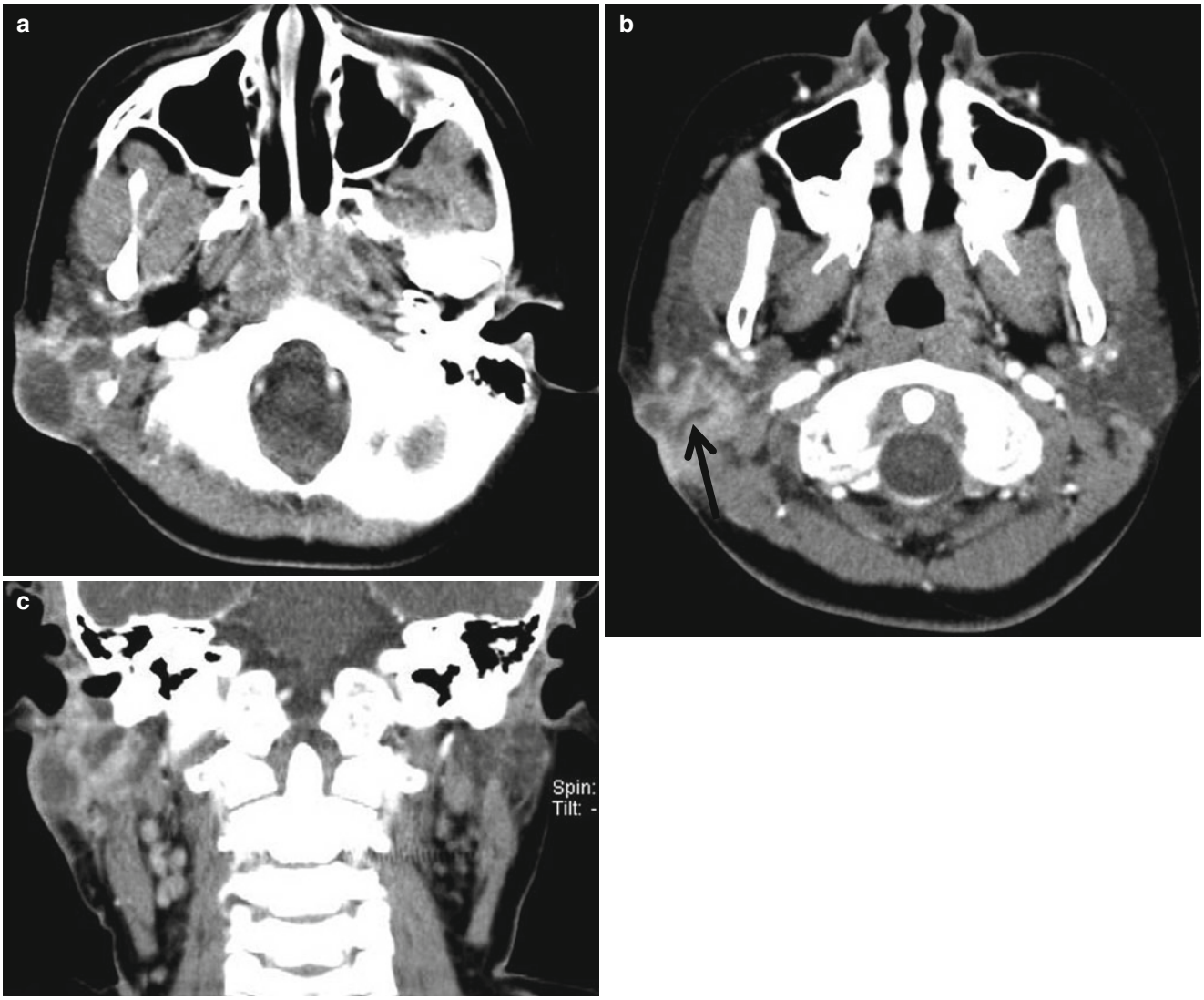

Fig. 7.11 First branchial cleft cyst in an 11-year-old girl. (**a**, **b**) Axial CT scans show a complicated, thick-walled cystic mass in the right infra-auricular soft tissue layer with a fine sinus tract (*arrow*). (**c**) Coronal reformatted CT scan shows the cystic mass extending just below the ear

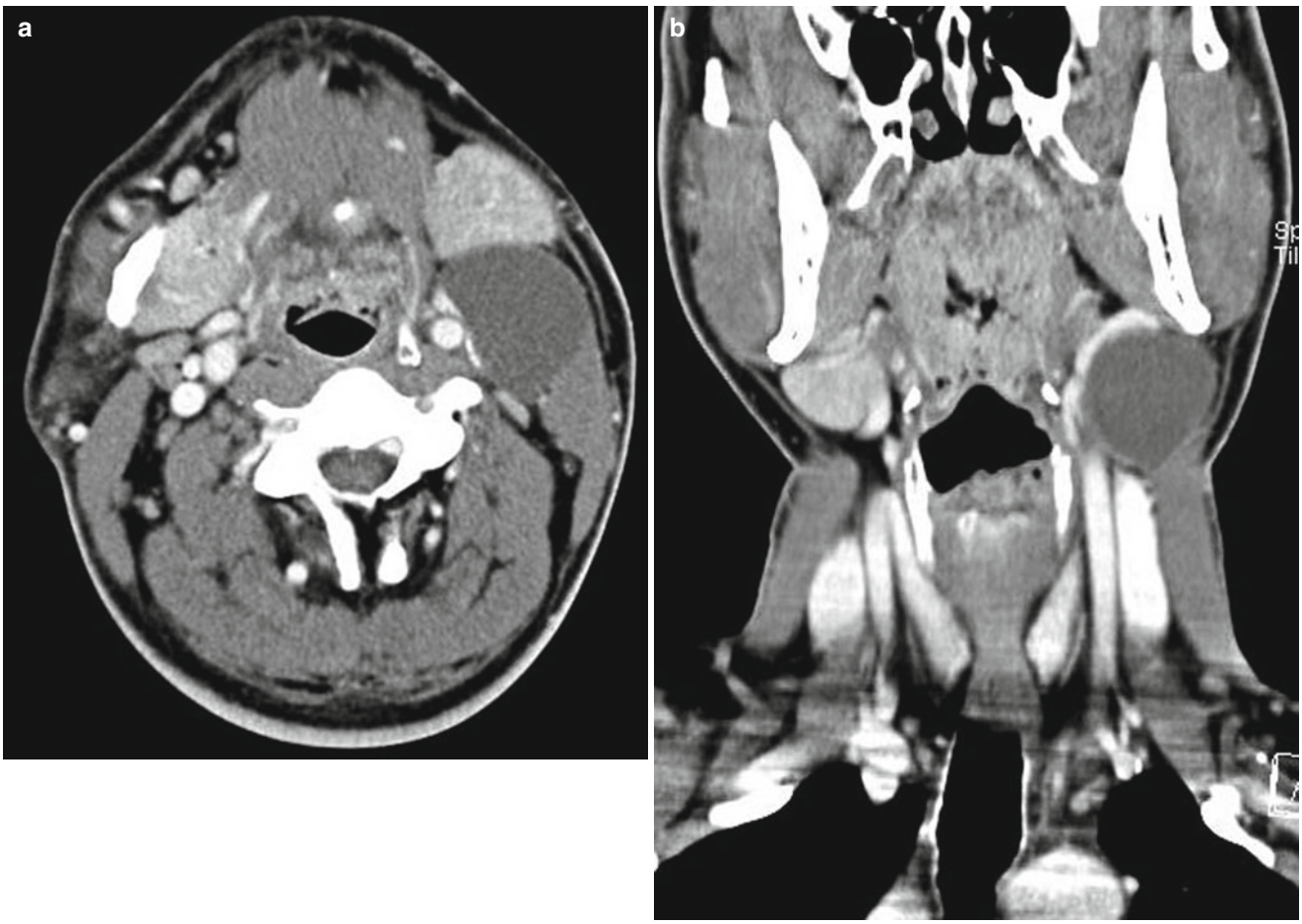

Fig. 7.12 Second branchial cleft cyst in an 18-year-old girl. (**a**) Axial CT scan shows a thin-walled mass with water attenuation in anteromedial to the sternocleidomastoid muscle. Note the anteriorly displaced submandibular gland, medially displaced left carotid sheath, and posteriorly displaced sternocleidomastoid muscle. (**b**) Coronal reformatted CT scan shows the typical location of the elongated cyst at the angle of the mandible

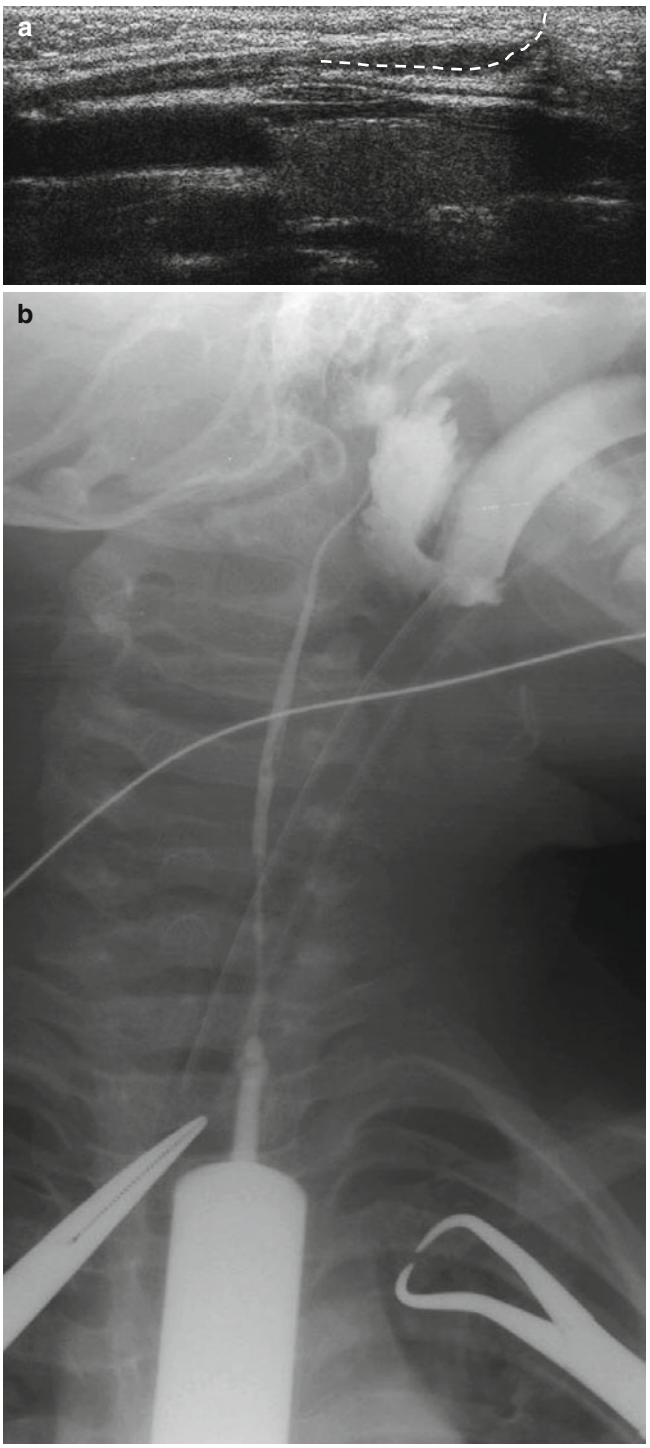

Fig. 7.13 Second branchial cleft fistula in a 2-year-old boy. (**a**) Longitudinal US of the neck shows a long, linear sinus (----) from the tiny skin pit on the anterior border of distal sternocleidomastoid muscle. US has a limited role for tracing the entire length of the sinus tract. (**b**) Operative sinogram shows the complete fistula tract extending from the skin pit in the lower neck to the right tonsillar fossa

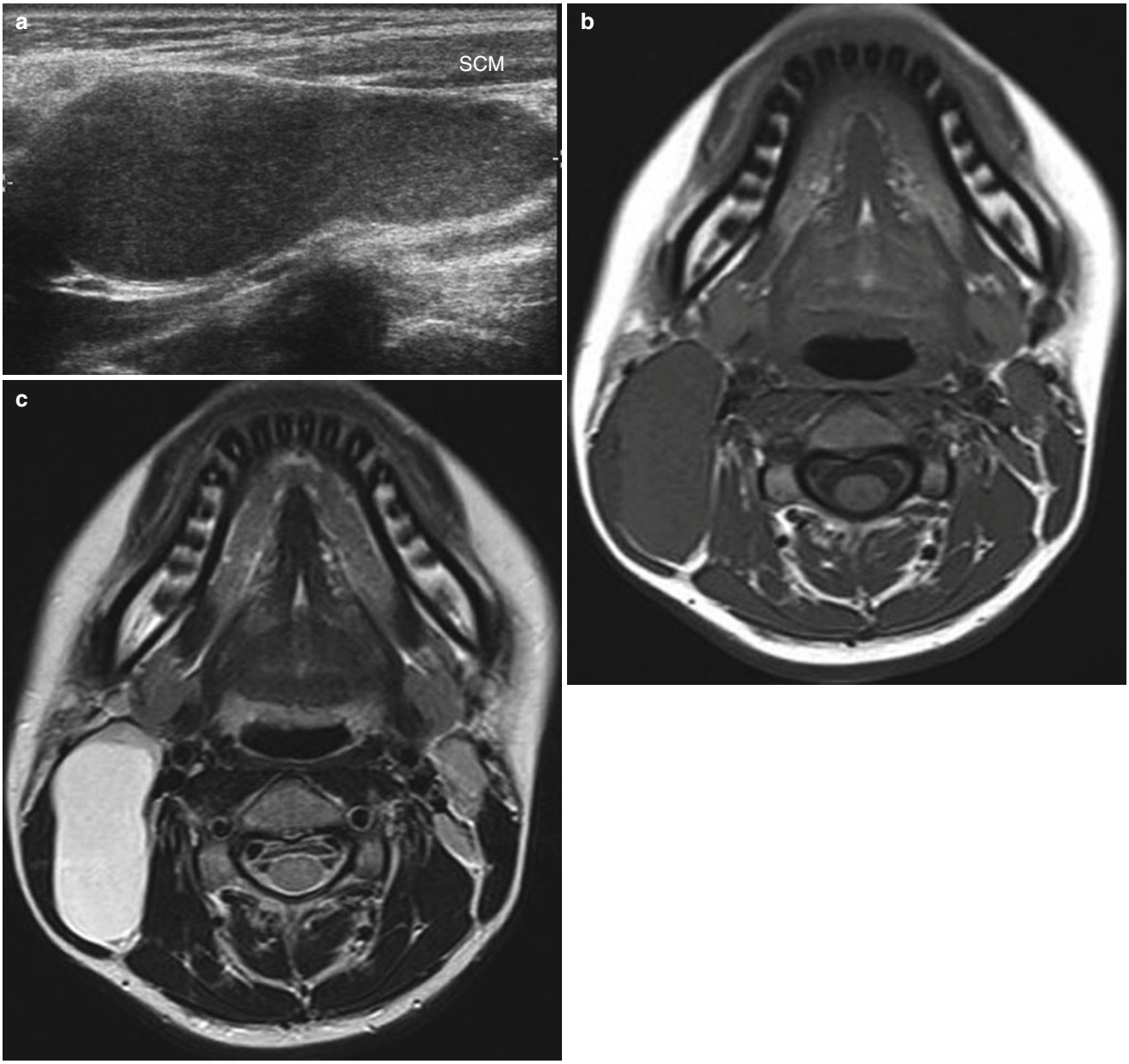

Fig. 7.14 Third branchial cleft cyst in a 16-year-old girl. (**a**) US shows an elongated cyst along the posterior aspect of the right sternocleidomastoid (SCM) muscle. Note the internal echogenic debridements indicating complicated or proteinaceous content. (**b**) Axial T1-weighted image shows an elongated cyst of isosignal intensity. (**c**) Axial T2-weighted image shows the cyst of high signal intensity, posterolateral to the carotid sheath, displacing the sternocleidomastoid muscle anterolaterally

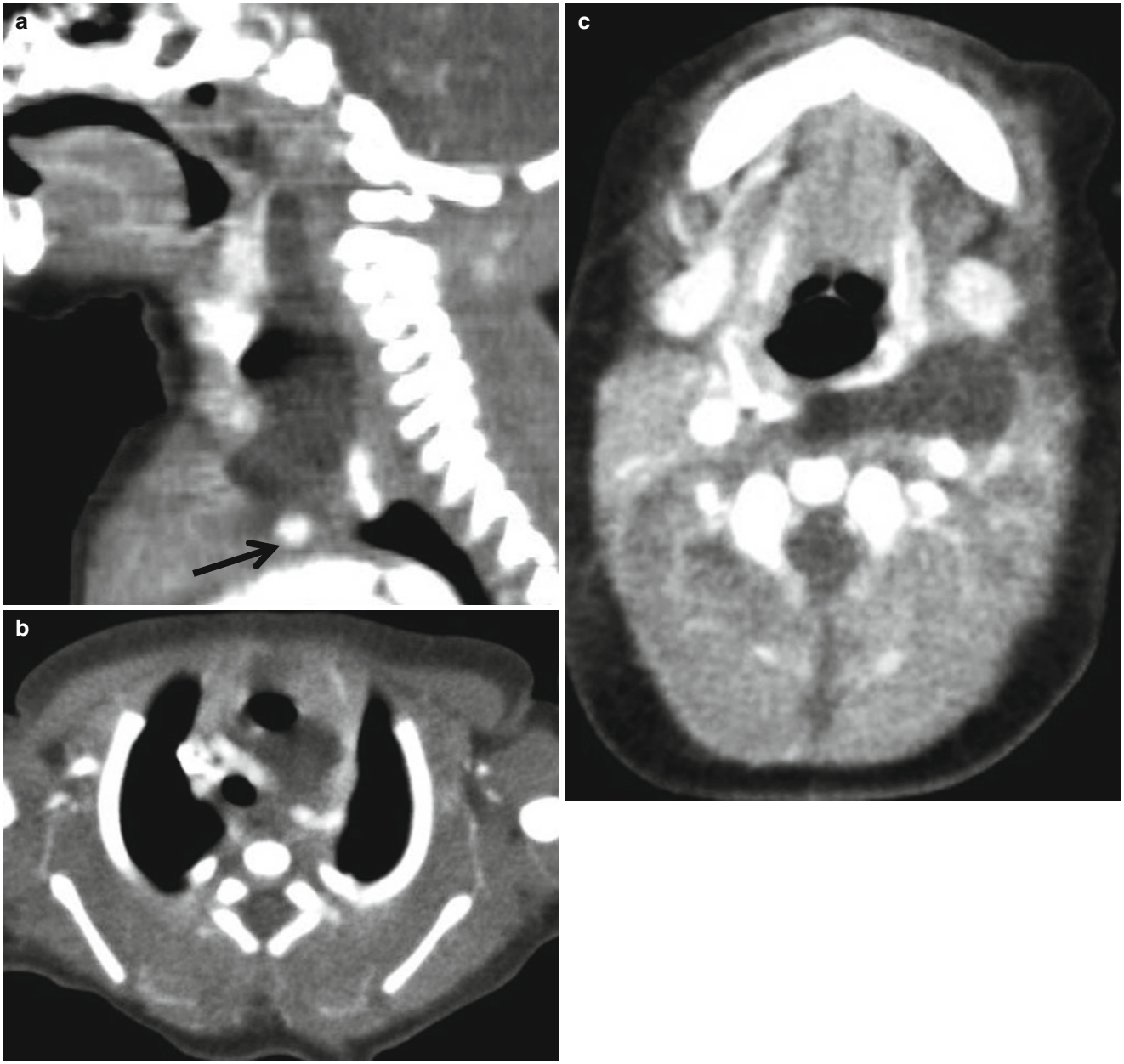

Fig. 7.15 Fourth branchial cleft cyst with a sinus in a 2-day-old neonate. (**a**) Contrast-enhanced sagittal reformatted CT scan shows a large air-containing elongated cystic mass from the hypopharynx to the level of the aortic arch (*arrow*). Note the motion artifact due to severe respiratory difficulty. (**b**, **c**) Contrast-enhanced axial CT scans show that the cyst is located anterior to the aortic arch and extends to the level of the pyriform sinus. Sinogram was not performed due to severe respiratory difficulty

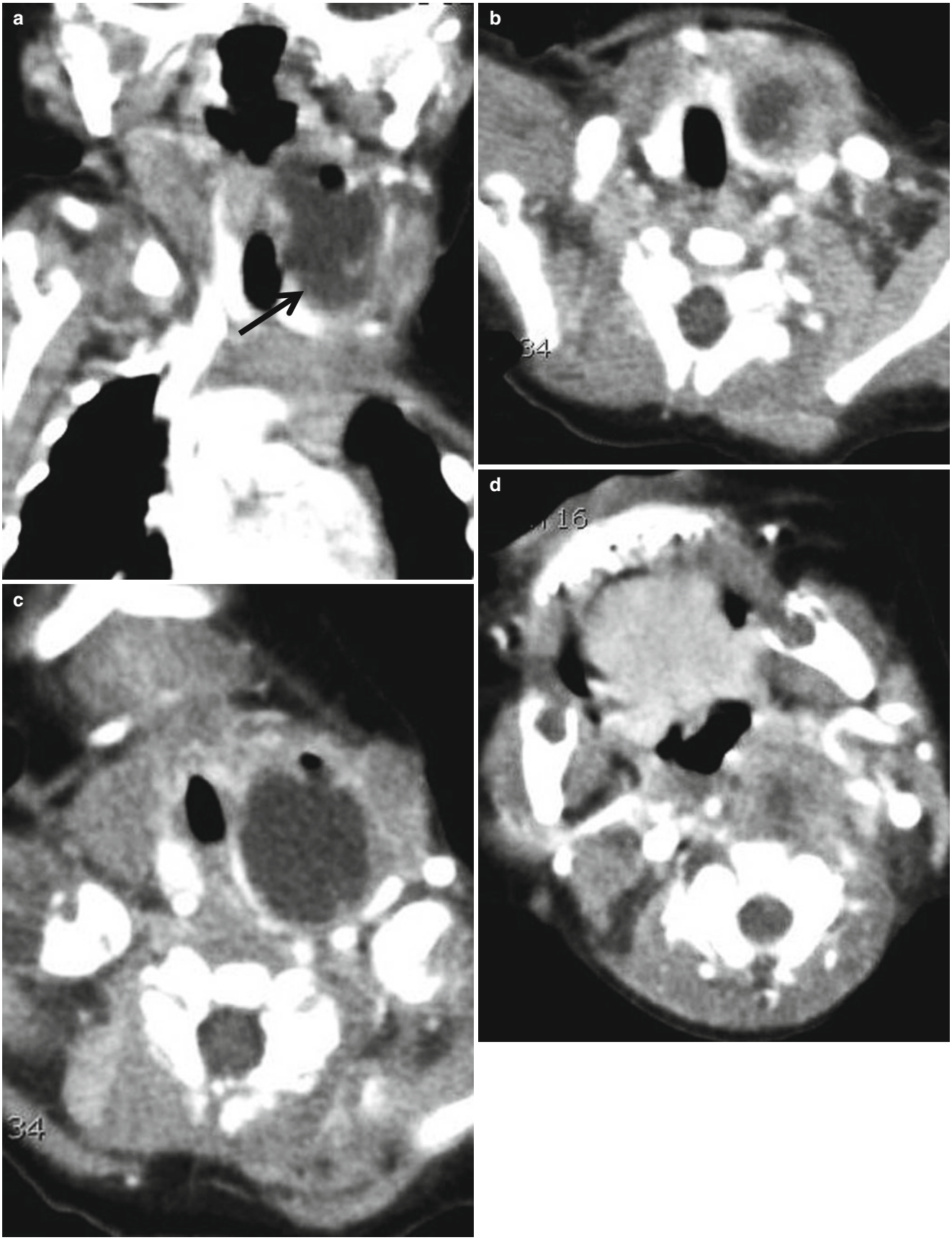

Fig. 7.16 Fourth branchial cleft cyst with a sinus in a 2-month-old infant. (**a**) Coronal reformatted CT scan shows an air-containing elongated cystic mass from the level of the pyriform sinus to the left low neck abutting the left thyroid gland (*arrow*). (**b–d**) Contrast-enhanced axial CT scans show the cyst abutting the left thyroid gland with internal air pocket and diffuse inflammatory change in the sternocleidomastoid muscle and left hypopharynx. (**e**) Esophagogram shows a faint linear sinus tract from the tip of the left pyriform sinus (*arrow*)

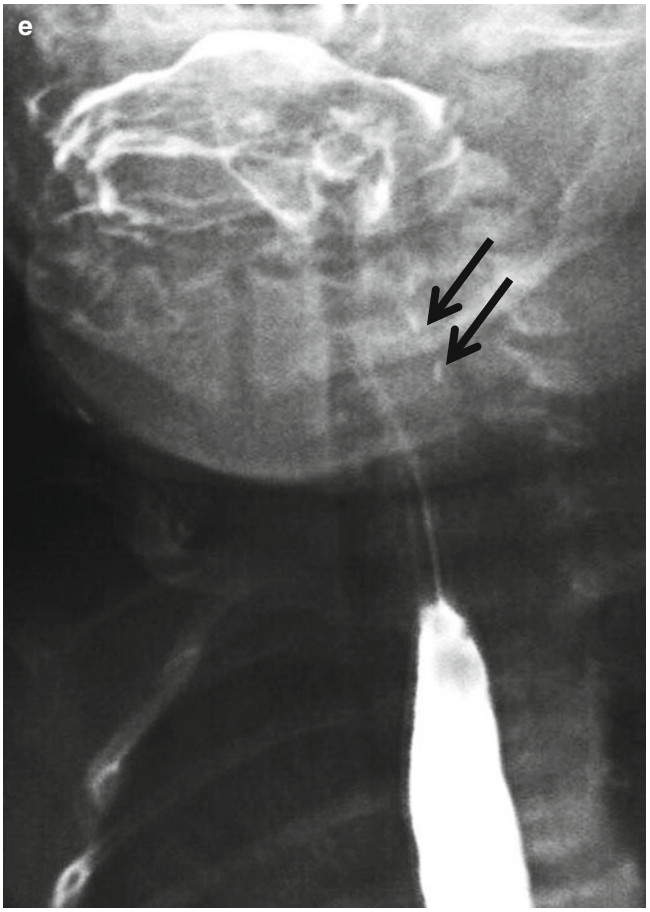

Fig. 7.16 (continued)

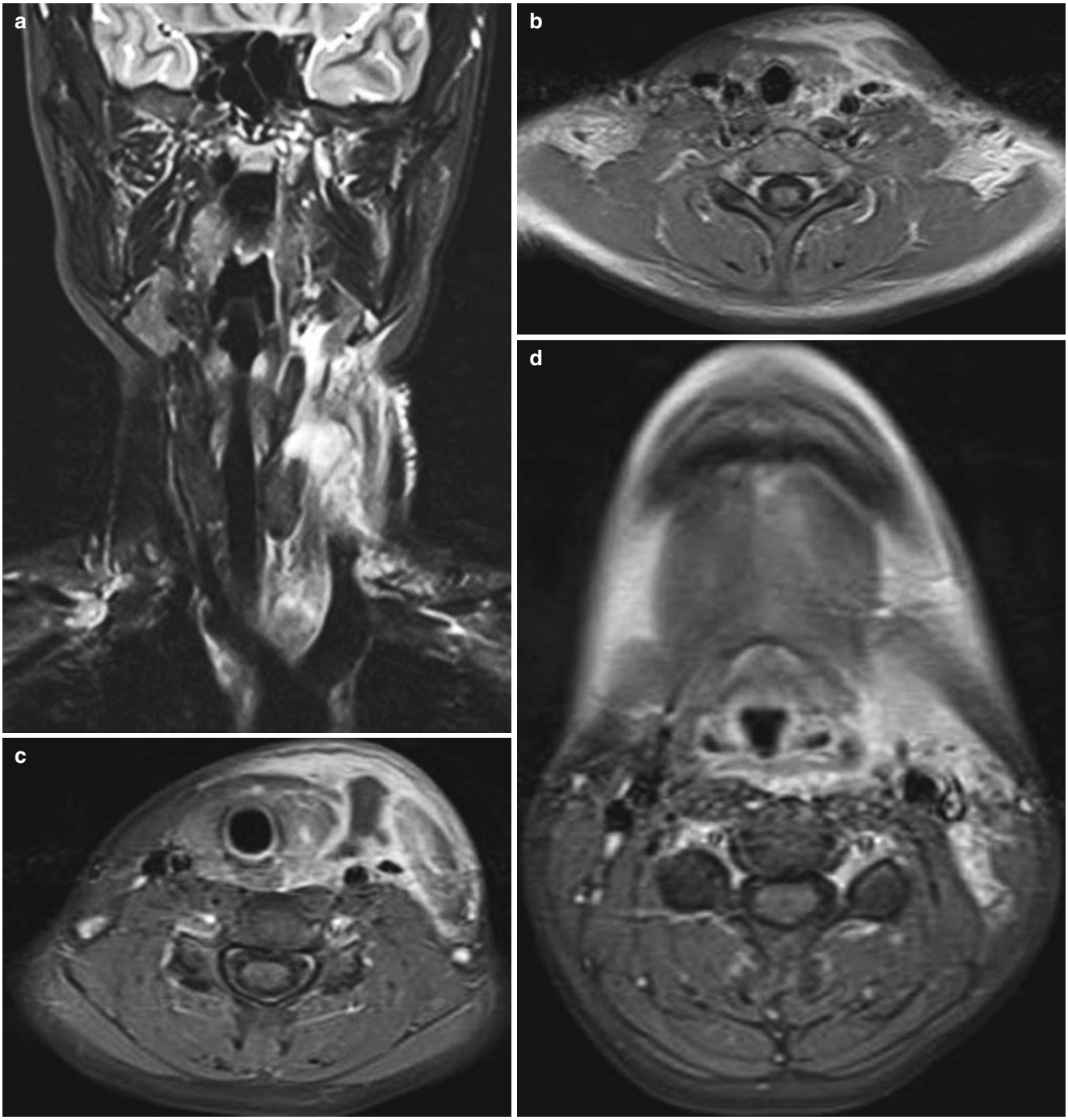

Fig. 7.17 Fourth branchial cleft sinus in a 13-year-old girl with a history of recurrent swelling on the left side of the neck. (**a**) Coronal T2-weighted MR image shows diffuse high signal intensity of soft tissue edema from the level of the pyriform sinus to the level of the aortic arch on the left. (**b**–**d**) Contrast-enhanced axial T1-weighted images show swelling of the left sternocleidomastoid muscle (**b**), left thyroid gland with perithyroidal abscess (**c**), and soft tissue inflammation around the hypopharynx (**d**). (**e**) Esophagogram shows a linear sinus tract from the tip of the left pyriform sinus (*arrow*)

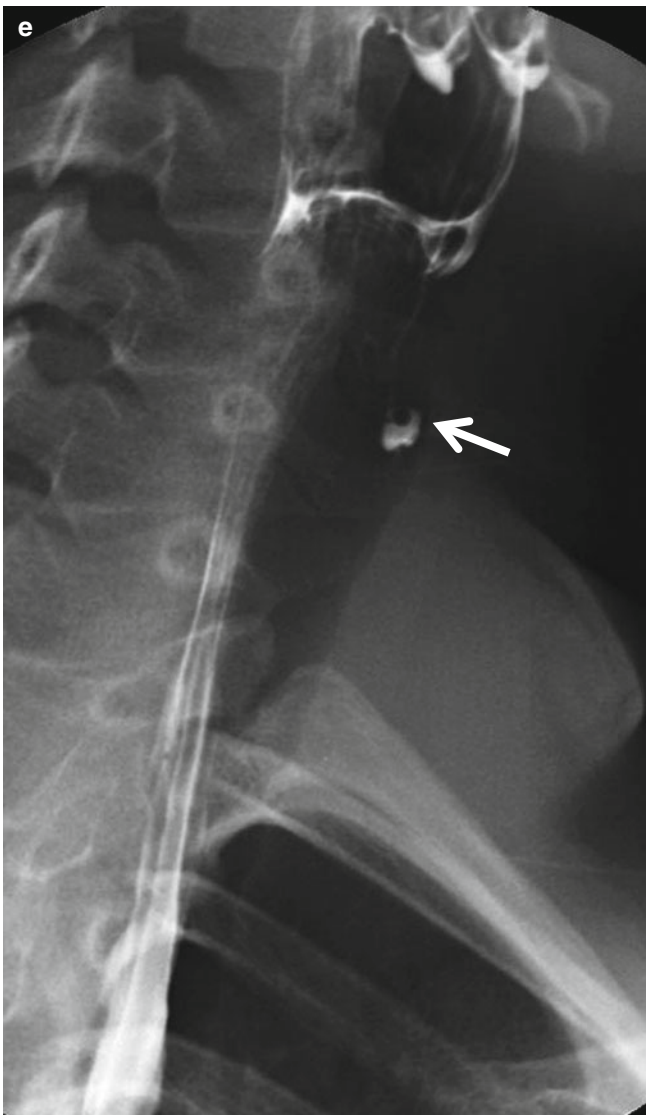

Fig. 7.17 (continued)

7.5.7 Thymic Anomalies

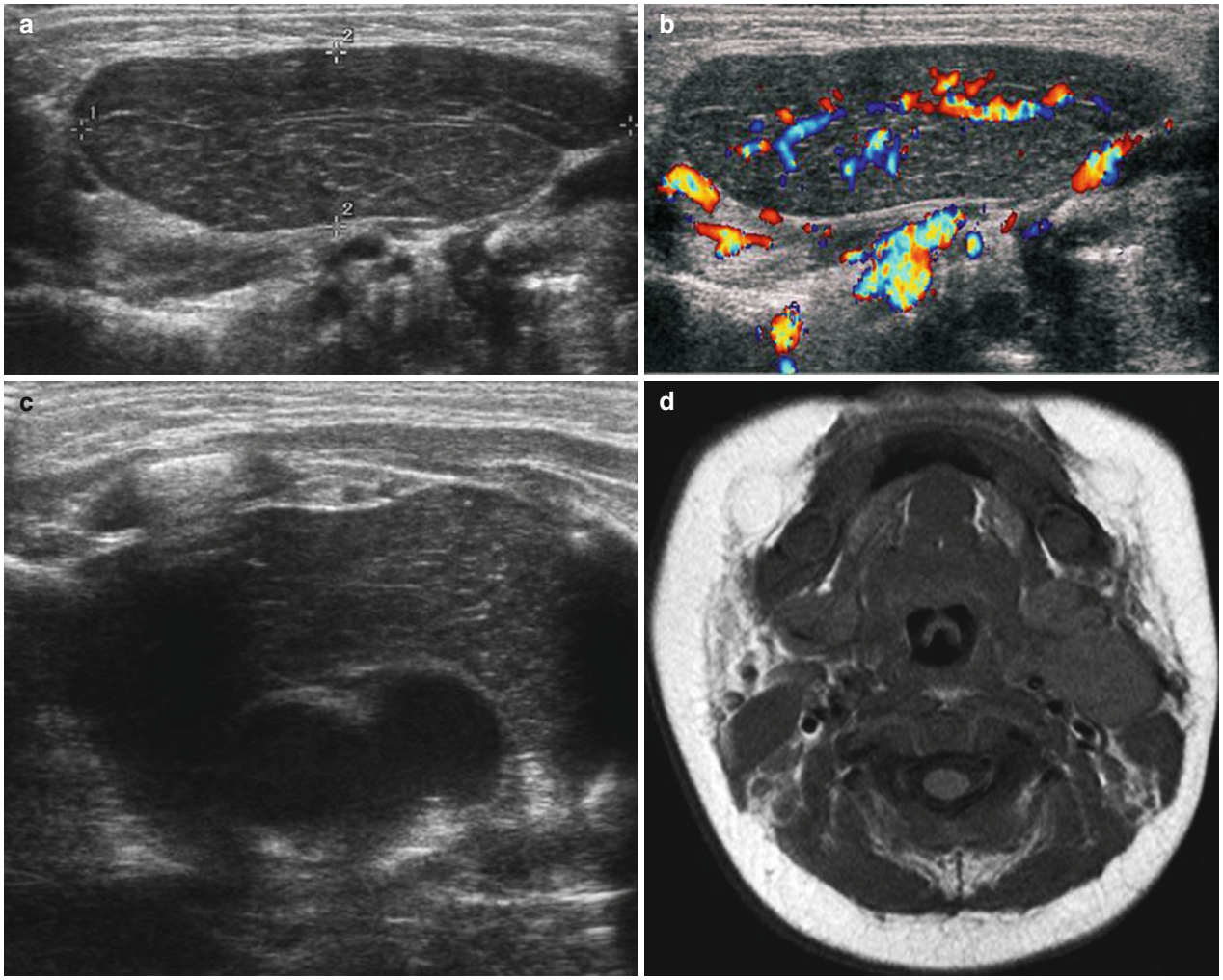

Fig. 7.18 Ectopic cervical thymus in a 12-week-old infant. (**a**) US shows a well-defined homogeneous, hypoechoic solid mass in the left anterior deep cervical space. (**b**) Color Doppler US shows minimal arterial and venous flow within the mass. (**c**) US also shows the same natured normal thymus in the anterior mediastinum. (**d**, **e**) Axial MR images show homogeneous isosignal intensity of the mass relative to the submandibular gland and slightly high signal intensity relative to the muscle on both T1- (**d**) and T2-weighted (**e**) images. The mass is located posterior to the submandibular gland. (**f**, **g**) Contrast-enhanced fat-suppressed axial and coronal T1-weighted images reveal homogeneously enhancing ectopic thymus (*long arrow*), which is isointense relative to the mediastinal thymus (*arrows*). Note the different enhancements of the submandibular glands

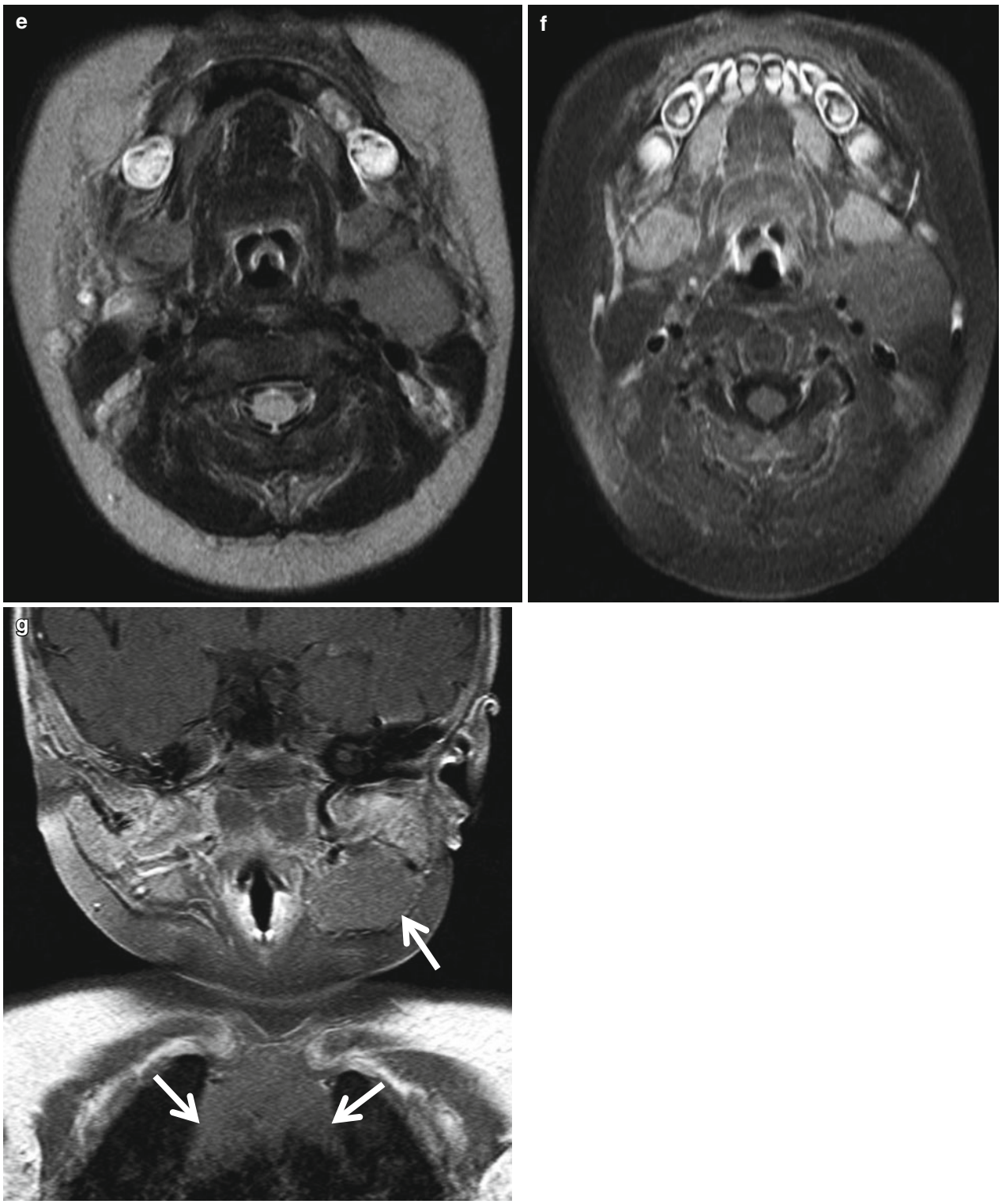

Fig. 7.18 (continued)

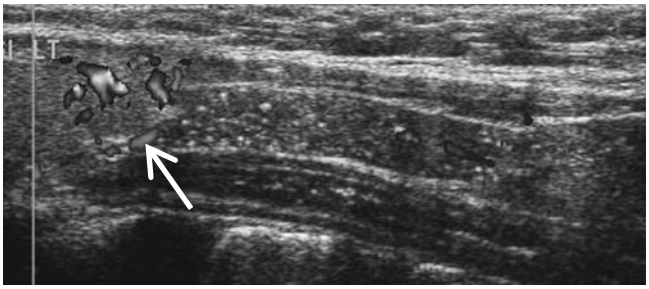

Fig. 7.19 Normal thymus with cervical extension in an 8-year-old boy. Longitudinal US scan of the left neck shows extension of the normal thymus from the anterior mediastinum to the low neck abutting the lower margin of the left thyroid gland (*arrow*). Note the "starry sky" appearance of the thymic parenchyma, which is thought to be hyperechoic fat against the background of the remaining hypoechoic lymphoid tissue

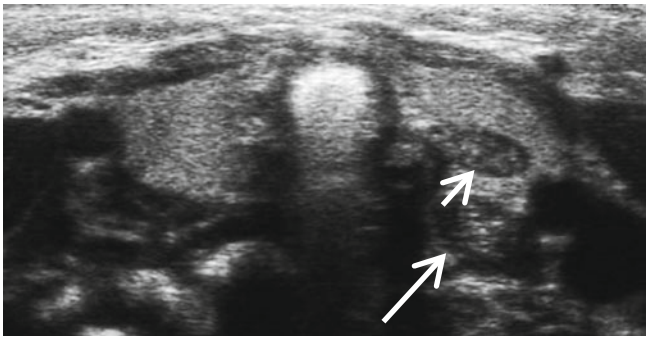

Fig. 7.20 Ectopic thymic tissue of the thyroid gland in a 4-day-old neonate. US shows a tiny low echoic solid nodule of ectopic thymus (*short arrow*), which shows the same echogenicity with the posteriorly located cervical thymus (*long arrow*) extending from the mediastinal thymus

7.5.8 Hypopharyngeal Cysts

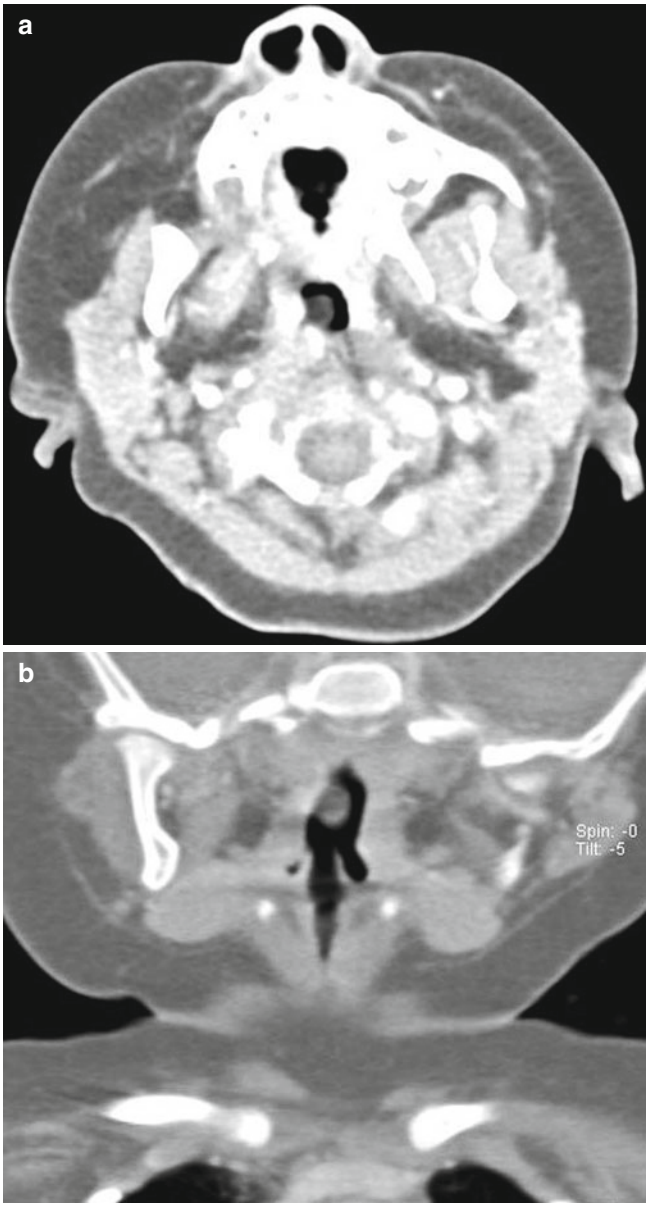

Fig. 7.21 Pharyngeal cyst in a 4-month-old infant. (**a**, **b**) CT scans of the neck show a small unilocular thin-walled cyst arising from the right lateral wall of the oropharynx

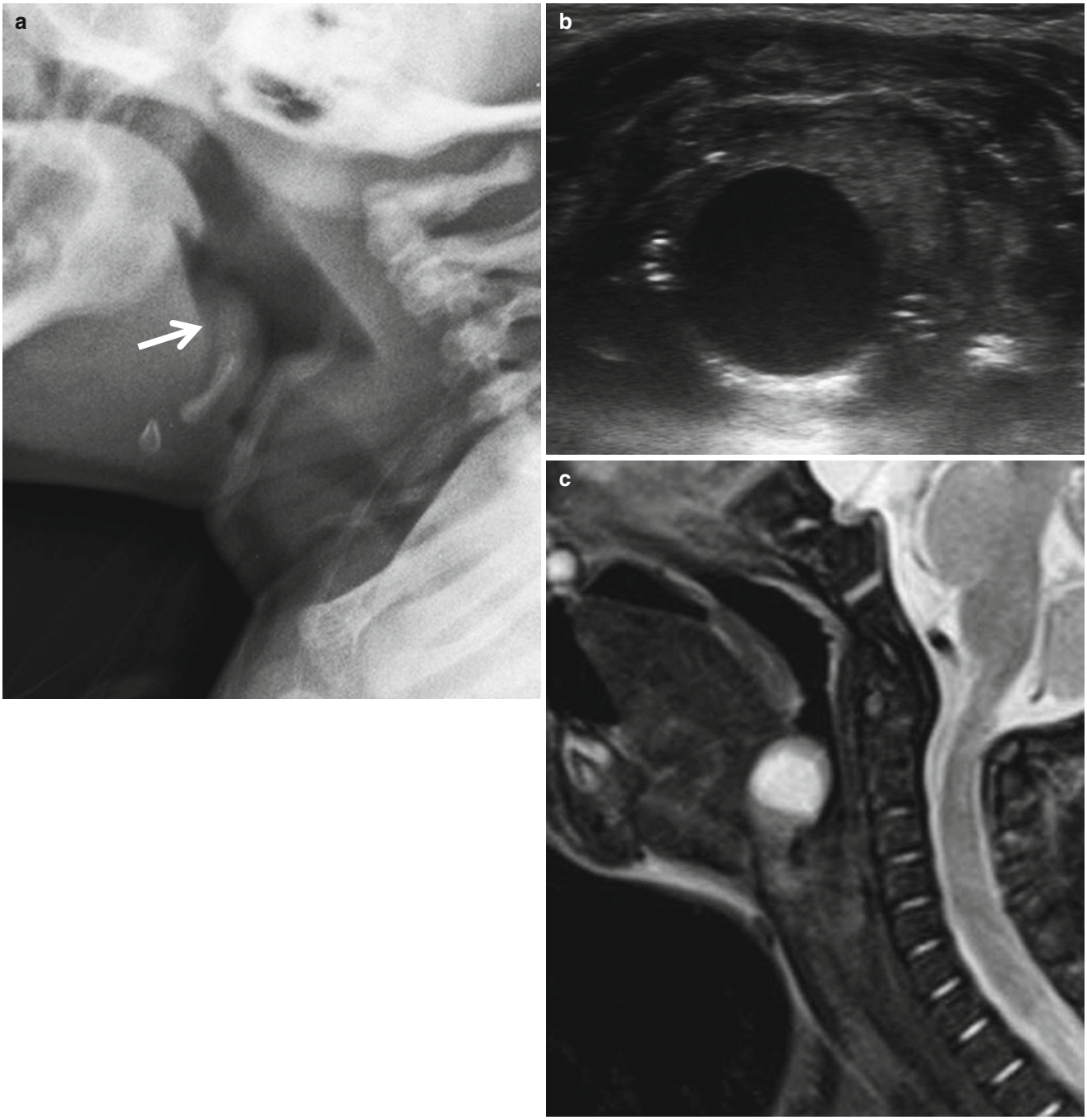

Fig. 7.22 Vallecular cyst in a 1-month-old infant. (**a**) Endolateral view of the neck shows a round soft tissue mass bulging into the anterior wall of the hypopharynx (*arrow*). (**b**) US shows a unilocular thin-walled cyst in the preepiglottic space. (**c**) Sagittal T2-weighted image shows a unilocular cyst of high signal intensity arising from the vallecula

Fig. 7.23 Vallecular cyst in a 1-month-old infant. (**a**) Endolateral view of the neck shows a round soft tissue mass bulging into the anterior wall of the hypopharynx. (**b**, **c**) Axial and coronal reformatted CT scans show a unilocular thin-walled cyst arising from the right lateral wall of the vallecula

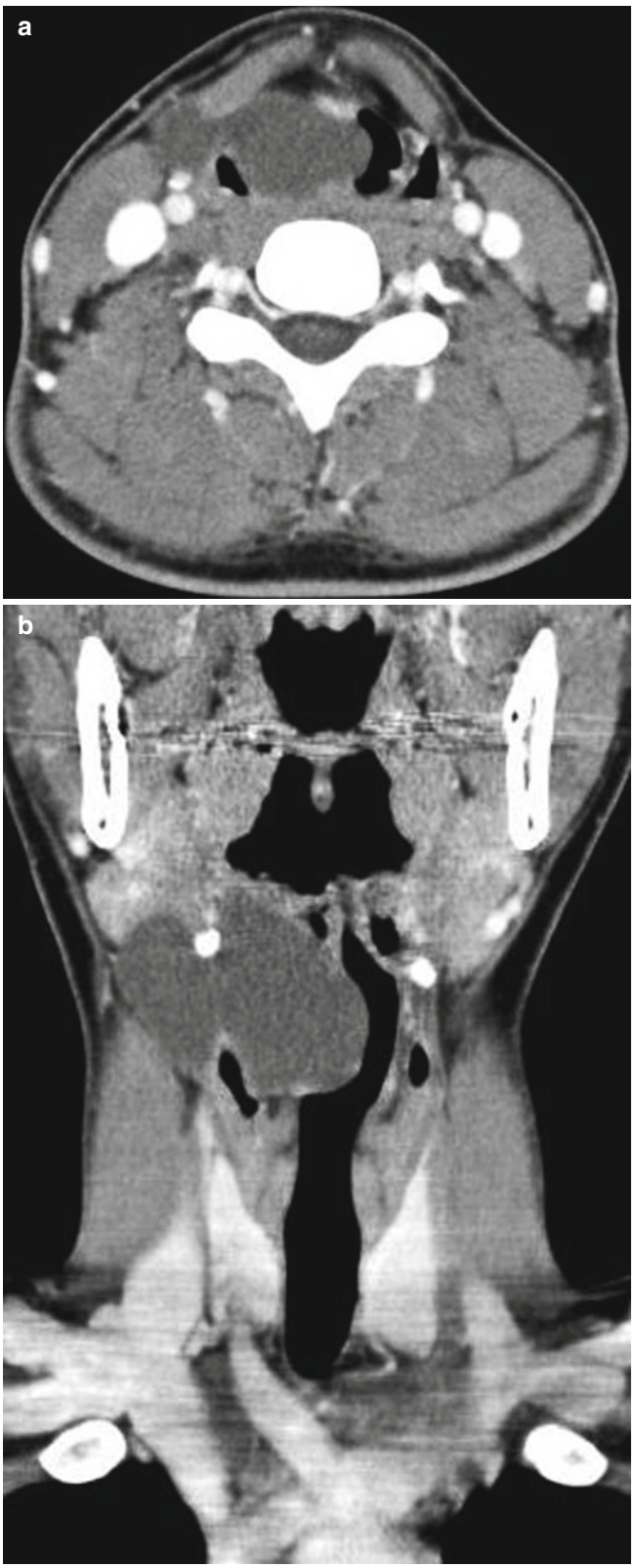

Fig. 7.24 Laryngocele in a 15-year-old boy. (**a**) Axial CT scan shows a bilobed cystic mass in the right lateral wall of the larynx. (**b**) Coronal reformatted CT scan shows a bilobed thin-walled cyst arising from the right lateral wall of the supraglottic larynx and extending into paralaryngeal soft tissue

7.5.9 Foregut Duplication Cysts

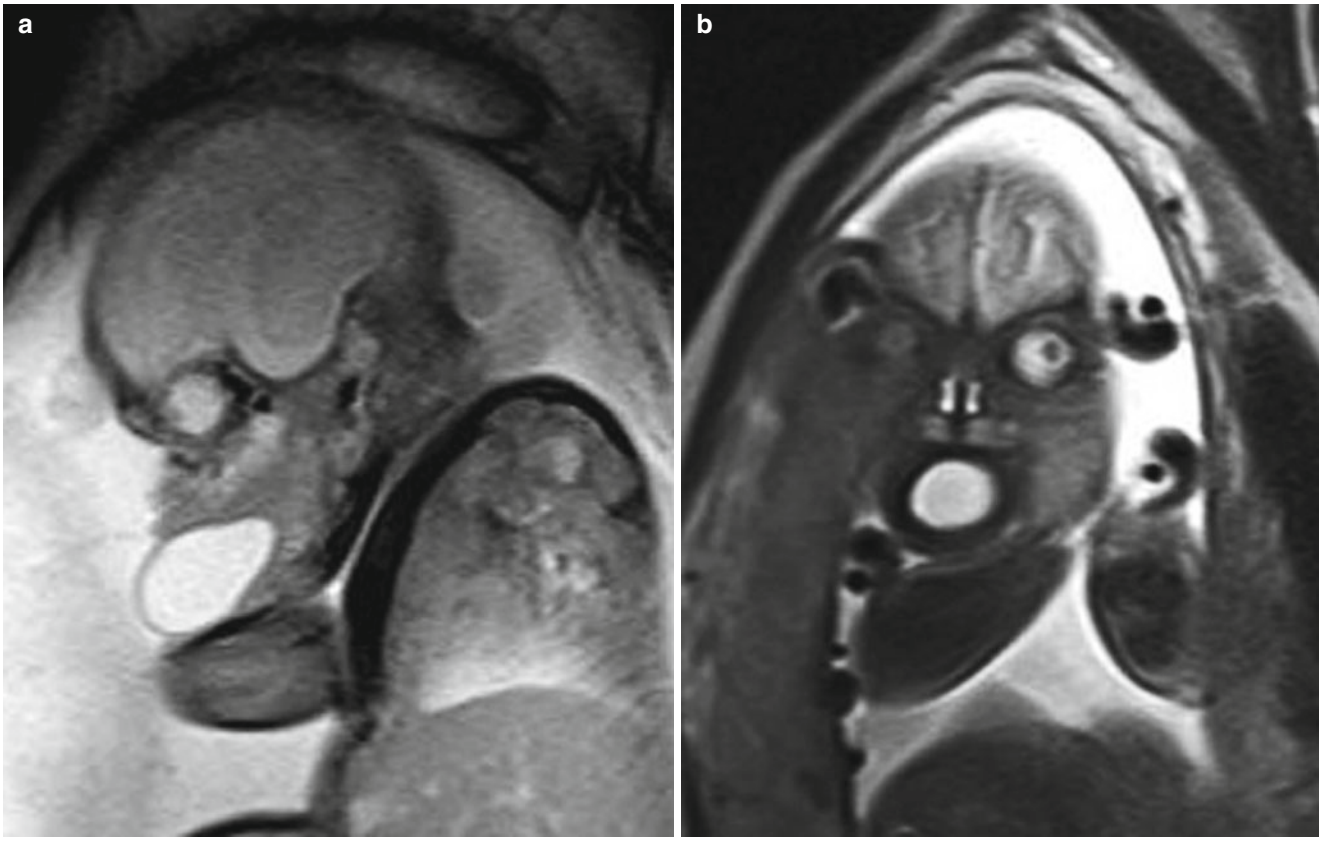

Fig. 7.25 Enteric duplication cyst in a fetus. (**a**) Sagittal T2-weighted MR image shows an oval-shaped cystic mass occupying the anterior two-thirds of the fetal mouth. (**b**) Axial and T2-weighted image shows the cystic mass in the fetal mouth

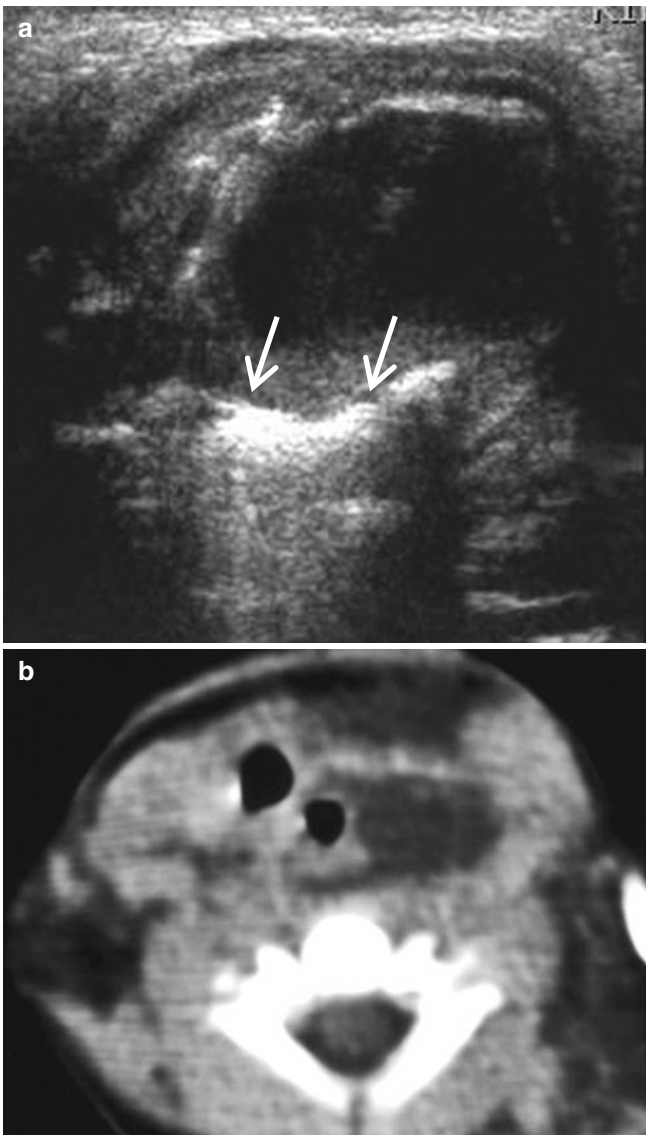

Fig. 7.26 Enteric duplication cyst in a 1-month-old infant. (**a**) US shows a thick-walled cyst in the left lateral aspect of the esophageal gas (*arrows*). (**b**) Axial CT scan shows a unilocular cyst abutting the left lateral wall of the esophagus

7.5.10 Vascular Malformations

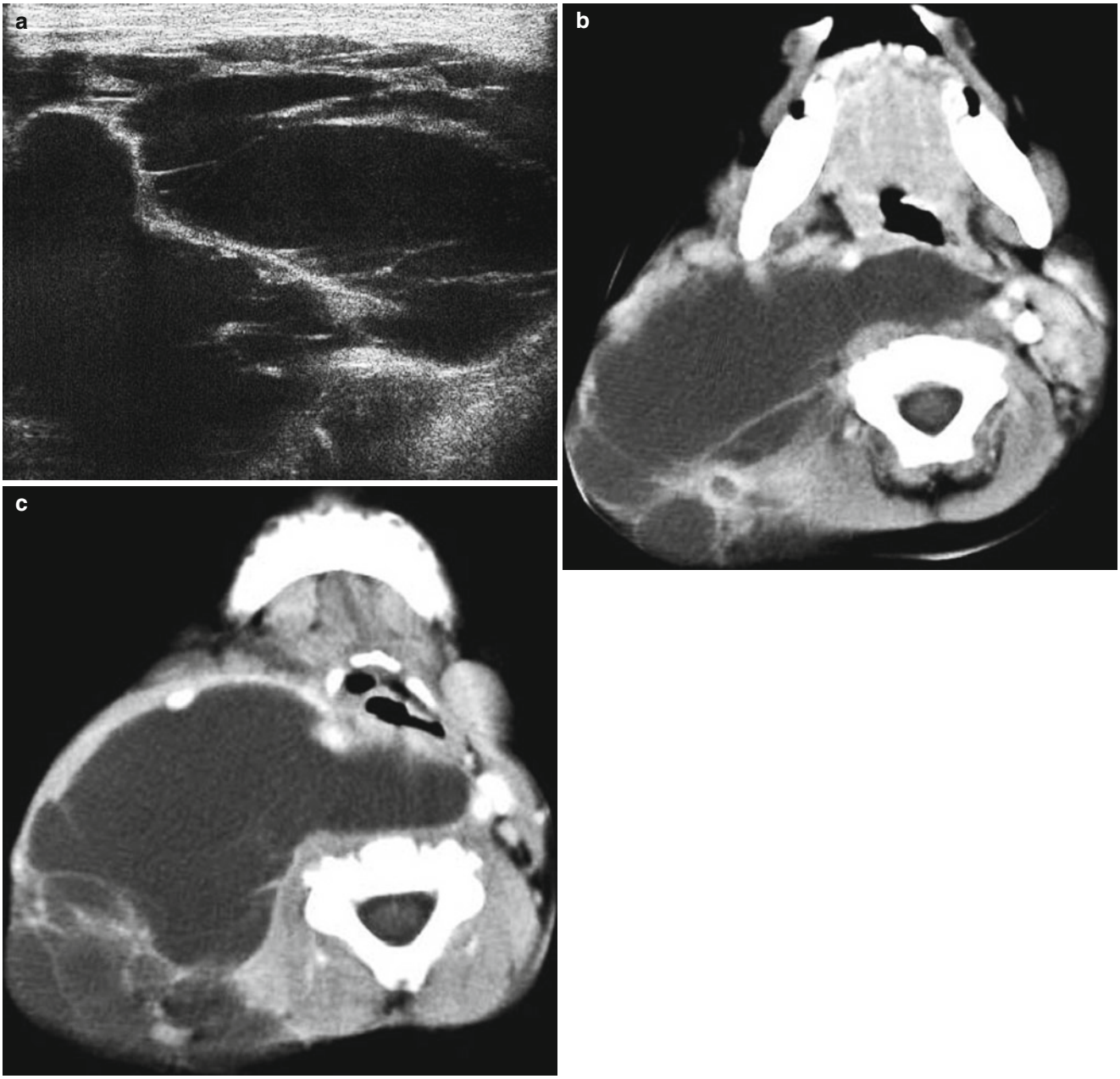

Fig. 7.27 Lymphangioma in a 1-year-old infant. (**a**) US shows a large, thin-walled multiseptated cystic mass. (**b**, **c**) Contrast-enhanced CT scans show a huge, multiseptated, thin-walled cystic mass in the posterior deep cervical space insinuating into the retropharyngeal space. Note the anteriorly displaced right sternocleidomastoid muscle

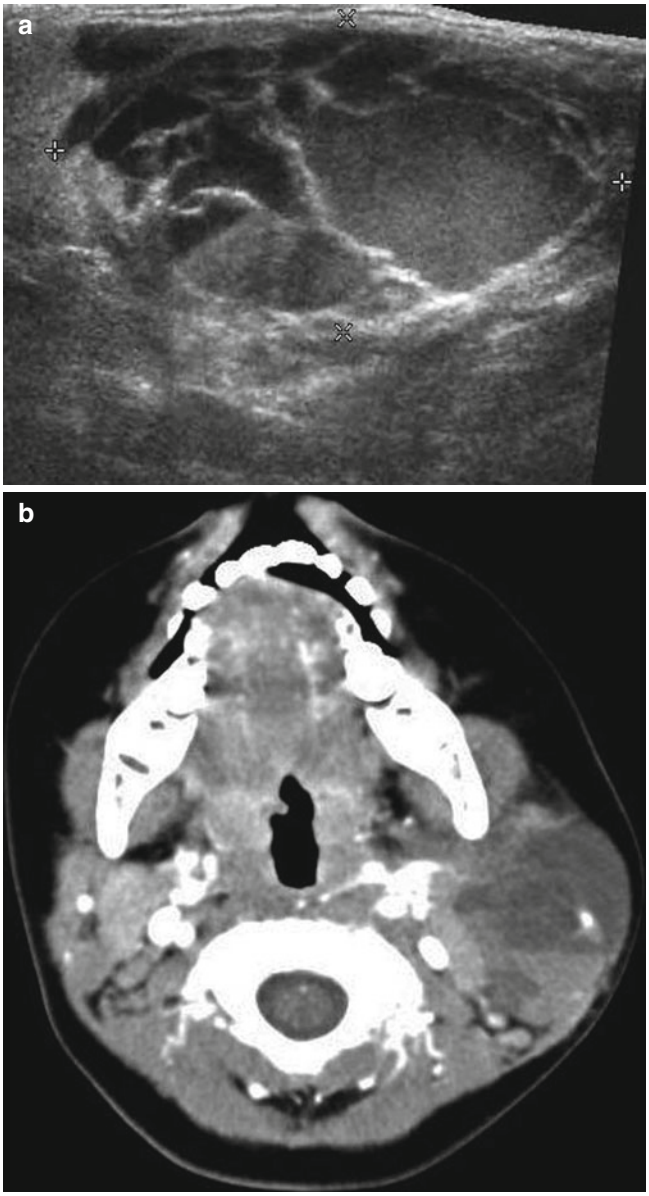

Fig. 7.28 Lymphangioma of the parotid gland in a 22-month-old boy. (**a**) US shows a multiseptated cystic mass with internal debridement in some of the chambers. (**b**) Contrast-enhanced axial CT scan shows a large, thin-walled, multiseptated mass with fluid–fluid levels in the left parotid gland

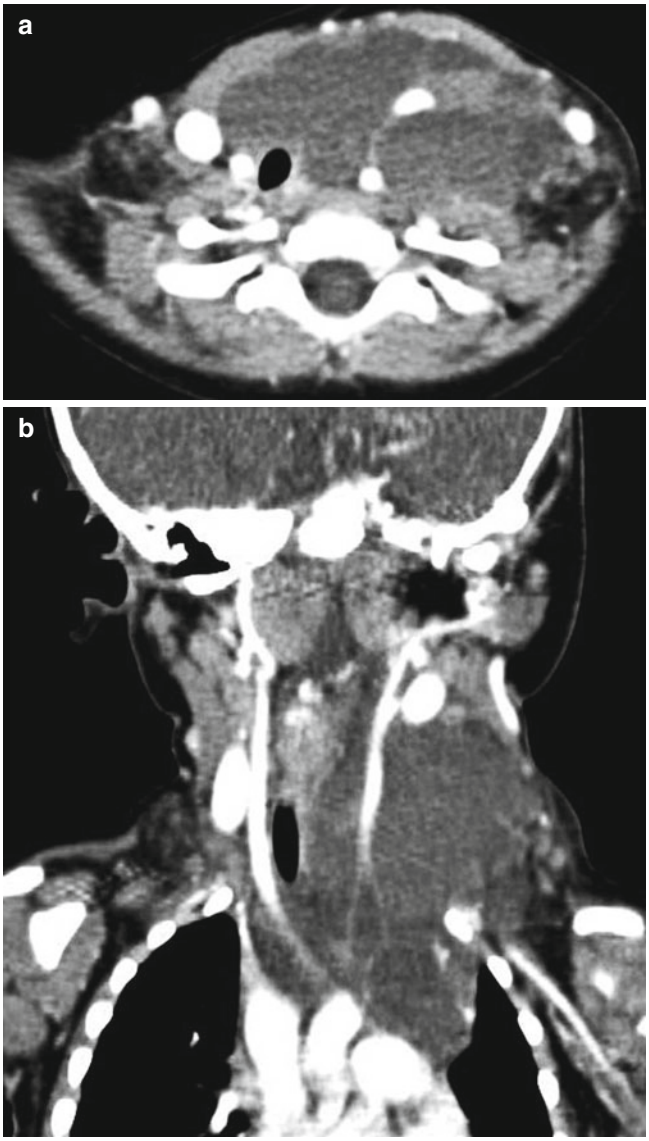

Fig. 7.29 Lymphangioma in a 10-month-old infant. (**a**, **b**) Contrast-enhanced axial and coronal CT scans show a huge, multilocular cystic mass involving the pretracheal and posterior deep cervical spaces with fluid–fluid levels and extending to the mediastinum. Note the mass insinuating around the vessels

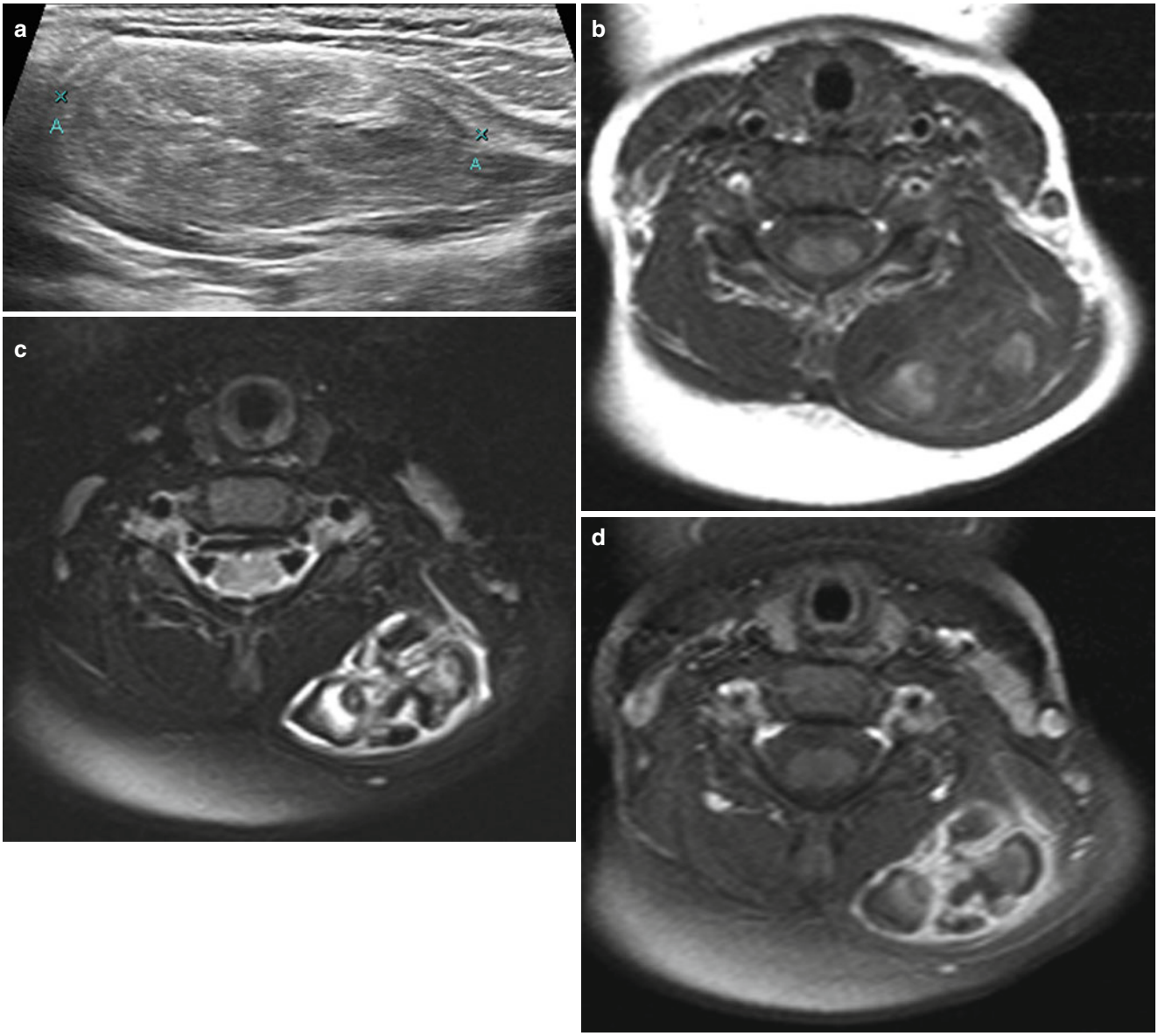

Fig. 7.30 Venous malformation in a 18-month-old girl. (**a**) US shows a heterogeneous complex mass (A) in the left posterior neck. (**b**, **c**) Axial T1- and fat-saturated T2-weighted images shows internal hemorrhage of variable signal intensities in the mass.(**d**) Contrast-enhanced fat-saturated axial T1-weighted image shows thick-walled enhancement of the septa

References

Baker LL, Dillon WP, Hieshima GB, et al. Hemangiomas and vascular malformations of the head and neck: MR characterization. Am J Neuroradiol. 1993;4:307–14.

Benson MT, Dalen K, Mancuso AA, et al. Congenital anomalies of the branchial apparatus: embryology and pathologic anatomy. Radiographics. 1992;12:943–60.

Chung PS, Chung YW, Park SJ, et al. A clinicopathologic study of epiglottic and vallecular cysts. Korean J Otorhinolaryngol. 2004;47:157–60.

Cigliano B, Baltogiannis N, Marco MD, et al. Cervical thymic cysts. Pediatr Surg Int. 2007;23:1219–25.

Gimm O, Krause U, Wessel H, et al. Ectopic intrathyroidal thymus diagnosed as a solid thyroid lesion: case report and review of the literature. J Pediatr Surg. 1997;32:1241–3.

Kieran SM, Robson CD, Nose V, et al. Foregut duplication cysts in the head and neck. Presentation, diagnosis, and management. Arch Otolaryngol Head Neck Surg. 2010;136:778–82.

Koeller KK, Alamo L, Adair CF, et al. Congenital cystic masses of the neck: radiologic-pathologic correlation. Radiographics. 1999; 19:121–46.

Lowe LH, Booth TN, Joglar JM, et al. Midface anomalies in children. Radiographics. 2000;20:907–22.

Morón FE, Morriss MC, Jone JJ, et al. Lumps and bumps on the head in children: use of CT and MR imaging in solving the clinical diagnostic dilemma. Radiographics. 2004;24:1655–74.

Mulliken JB, Glowacki J. Hemangiomas and vascular malformations in infants and children: a classification based on endothelial characteristics. Plast Reconstr Surg. 1982;69:412–22.

Nasseri F, Eftekhari F. Clinical and radiologic review of the normal and abnormal thymus: pearls and pitfalls. Radiographics. 2010; 30:413–28.

Sadler TW. Head and neck. In: Sadler TW, (ed) Langman's medical embryology, 12th ed. Baltimore: Williams and Wilkins; 2012.

Smirniotopoulos JG, Chiechi MV. Teratomas, dermoids, and epidermoids of the head and neck. Radiographics. 1995;15:1437–55.

Som PM, Smoker WRK, Curtin HD, et al. Congenital lesions of the neck. In: Som PM, Curtin HD, editors. Head and neck imaging. 4th ed. St. Louis: Mosby; 2003.

Suzuki J, Hashimoto S, Watanabe K, et al. Congenital vallecular cyst in an infant: case report and review of 52 recent cases. J Laryngol Otol. 2011;125:1199–203.